**Title: A NANOG-pERK reciprocal regulatory circuit mediates *Nanog* autoregulation and ERK signaling dynamics.**

**Author line:**
Hanuman T Kale, Rajendra Singh Rajpurohit, Debabrata Jana, Vishnu V Vijay, Mansi Srivastava, Preeti R Mourya, Gunda Srinivas, P Chandra Shekar*

CSIR-Centre for Cellular and Molecular Biology, Uppal Road, Hyderabad, Telangana, India 500007.

*Correspondence: csp@ccmb.res.in

**The self-renewal and differentiation potential of Embryonic stem cells (ESCs) is maintained by the regulated expression of core pluripotency factors. The expression level of core pluripotency factor *Nanog* is tightly regulated by a negative feedback autorepression loop. However, it remains unclear how the ESCs perceive the NANOG levels and execute autorepression. Here, we show that a dose-dependent induction of *Fgfbp1* and *Fgfr2* by NANOG activates an autocrine mediated ERK signaling in high-*Nanog* cells to trigger autorepression. pERK recruits NONO to *Nanog* locus to repress transcription by preventing POL2 loading. The *Nanog* autorepression process establishes a self-perpetuating NANOG-pERK reciprocal regulatory circuit. We further demonstrate that the reciprocal regulatory circuit induces the pERK heterogeneity and ERK signaling dynamics in pluripotent stem cells.**

Embryonic stem (ES) cells are characterized by long-term self-renewal and the potential to differentiate to all cell types of the germ layers. ES cells cultured in presence of serum and LIF manifest transcriptional and functional heterogeneity. The heterogeneous expression of transcription factors like *Nanog*, *Rex1*, *Stella*, *Esrrb*, *Klf4,* and *Tbx3* determine differential fate choice(1-9). The core pluripotency factor, *Nanog* was identified as a factor conferring LIF independent self-renewal to ES cells by inhibiting differentiation(10, 11). *Nanog* switches between mono-allelic and bi-allelic expression during embryonic development and in alternate pluripotency states(3, 12). The expression of *Nanog* is restricted in ES cells to ensure their potential to differentiate by negative feedback autorepression and other repressive mechanisms(13-19). Among the multiple mechanisms that regulate *Nanog,* which mechanisms are utilized by the pluripotent cells to restrict *Nanog* by autorepression remain unknown Although *Nanog*

autorepression was shown to operate independently of OCT4/SOX2(16) and dependent on ZFP281(13), it is unclear how the NANOG protein levels are perceived by cells to trigger autorepression. Here, we show that ERK signaling is essential for *Nanog* autorepression. NANOG induces *Fgfr2* and *Fgfbp1* exclusively in the high-*Nanog* ESCs to trigger feedback repression by autocrine-mediated activation of ERK signaling. We show that pERK1/2 recruits NONO to the *Nanog* locus to repress *Nanog* transcription by affecting POL2 loading. We show that the Nanog autoregulation process results in a self-perpetuating NANOG-pERK reciprocal regulatory loop. Our results establish that the NANOG-pERK reciprocal regulatory loop is the basis of ERK signaling dynamics and pERK1/2 heterogeneity in pluripotent stem cells. Together with our data show that the NANOG-pERK axis may not merely be viewed as a mechanism to regulate *Nanog*, but also a mechanism by which ERK dynamics and heterogeneity is induced in the pluripotent cells.

## Results

### Residual MEK1/2 activity in the ground state prevents complete derepression of *Nanog*.

Transcriptional regulation is the major mechanism regulating *Nanog* heterogeneity, biallelic expression, and autorepression(13). To uncouple the influence of MEK1/2 and GSK3$\beta$ on *Nanog* expression in naïve state of pluripotency, we analyzed the activity of *Nanog* promoter reported by GFP in TβC44Cre6 cell line(1) in combinations of MEK1/2 and GSK3$\beta$ inhibitors. TβC44Cre6 cell line is *Nanog* null ESC in which a Neomycin resistance cassette is knocked in into one allele of *Nanog* and GFP into another allele. *Nanog* expression was derepressed above the basal level (SL) in all treatments. *Nanog* promoter activity was higher in SLPD relative to 2iL (Fig. 1A). To analyze NANOG protein dynamics, we generated a NiRFP2A cell line with both endogenous alleles of Nanog expressing NANOG-IRFP fusion protein (Fig. S1A). Higher NANOGiRFP in SLPD (Fig. 1B), confirmed the highest induction of *Nanog* transcript and protein in SLPD. To dismiss the interference of genetic modifications in the *Nanog* locus on its expression(20); we analyzed its expression in E14Tg2a cells. The *Nanog* transcript (Fig. 1C), transcriptional activity (Fig. 1D), and protein (Fig. 1E) were highest in SLPD, unlike OCT4 protein which changed very little (Fig. 1C-E, Fig. S1B). SLPD and 2iL contain 1 $\mu$M PD, higher *Nanog* expression in SLPD indicated inefficient

repression of *Nanog* in 2iL/SL2i. We analyzed pERK1/2 to investigate possible modulation of MEK1/2 activity by GSK3$\beta$(21). The pERK1/2 remained undetectable for up to 4 hrs in SLPD and 2iL/SL2i. It gradually increased in 2iL after 8 hrs but remained undetectable in SLPD (Fig. 1F, Fig. S1C). The pERK1/2 in SLCHIR and 2iL significantly exceeded SL and SLPD respectively by 24 hrs (Fig. 1G, Fig. S1D), suggesting a long-term CHIR treatment enhanced MEK1/2 activity in ESCs. Further, the PD and CHIR dose-responsive experiments confirmed that the pERK1/2 positively correlated with the CHIR concentrations (Fig. 1H, I, Fig. S1E-H). Collectively, our data demonstrate that *Nanog* attains higher expression in MEK1/2 inhibition than in 2iL. GSK3$\beta$ activity negatively modulates MEK1/2 activity and its inhibition by CHIR increases pERK1/2 in 2iL over time.

**FGF autocrine signaling pathway components are essential for *Nanog* autoregulation.**

We asked if all repressive mechanisms including the *Nanog* autorepression are abolished in SLPD. We generated two NANOG restoration systems by integrating Flag-Avi-NANOG-ER$^{T2}$ (NANOGER$^{T2}$) and a Doxycycline-inducible Flag-Avi-NANOG (FaNANOG) transgene in Tβc44Cre6(1) to derive the TNERT and TDiN cell lines respectively (Fig. 2A, Fig. S2A, B). The repression of endogenous *Nanog*:GFP upon induction of transgenic NANOG by OHT/Dox is a functional readout of *Nanog* autoregulation. *Nanog*:GFP was repressed in OHT/Dox induced TNERT/TDiN in all treatments except SLPD (Fig. 2A, Fig. S2C, D). The data from distinct induction systems conclusively establish an essential role of MEK1/2 in *Nanog* autoregulation.

FGF signaling is the predominant inducer of MEK/ERK in pluripotent cells(22, 23), we investigated its role in autoregulation. NANOGER$^{T2}$/FaNANOG failed to repress *Nanog*:GFP in presence of FGFR inhibitor, suggesting an essential role of FGFRs (Fig. 2B, Fig. S2E). FGFR1, FGFR2, and FGF4 are major receptors and ligands of FGF signaling in early embryos(24, 25). FGFBP1 is a carrier protein expressed from early to late blastocyst (Fig. 2C)(26) that enhances FGF signaling(27). We deleted *Fgfr1*, *Fgfr2*, *Fgf4*, and *Fgfbp1* in TNERT cells to analyze their role in autoregulation (Fig. 2D, Fig. S2F-I). Except in TNERTFgfr1-/-, *Nanog*:GFP was not repressed in TNERTFgfr2-/-, TNERTFgf4-/- and TNERTFgfbp1-/- cells upon OHT induction (Fig. 2E). Our data suggest that FGF autocrine signaling and its components FGFR2, FGF4, and FGFBP1 are essential for *Nanog* autoregulation.

105

106 **NANOG enhances the expression of FGFR2, FGF4, and FGFBP1.**

107

108 We analyzed the expression of FGF autocrine signaling components during the
109 time course of OHT induction. *Fgf4, Fgfr2, Fgfr1,* and *Fgfbp1* transcripts were induced
110 within 1-2 hrs (Fig. 3A). Increased pre-mRNA indicated transcriptional activation of
111 these genes (Fig. 3B). ChIP-seq data analysis identified NANOG occupancy on *Fgf4,*
112 *Fgfbp1, Fgfr1,* and *Fgfr2*, which was further enhanced in *Oct4*+/- cells that have higher
113 NANOG (Fig. S3A)(28). To analyze the dosage-dependent occupancy of NANOG on
114 these genes, we generated EDiN cell line by introducing a Doxycycline-inducible
115 FaNANOG transgene in E14Tg2a. ChIP-PCR confirmed NANOG occupancy on *Fgf4*,
116 *Fgfbp1*, *Fgfr1*, and *Fgfr2*, which was further enhanced in PD (Fig. 3C) and EDiN+Dox
117 (Fig. 3D) which express higher NANOG. The data suggest a dose-dependent occupancy
118 of NANOG on the FGF signaling component genes. FGFR1, FGFR2, and pERK1/2 were
119 significantly increased upon OHT induction in TNERT (Fig. 3E). The strength of FGF
120 signaling depends on facilitation by carrier proteins(27), the affinity of ligands(29, 30)
121 and subsequent subcellular trafficking of the FGFRs(31, 32). The induction of
122 NANOGER$^{T2}$ enhanced FGFR2 on the cell surface (Fig. 3F), unlike the FGFR1 (Fig.
123 S3B) suggesting NANOG specifically enhances FGFR2. Intriguingly, FGFR2
124 expression exhibited a negatively skewed bimodal distribution resembling *Nanog*
125 expression(1) (Fig. 3F). The NANOGER$^{T2}$ induction increased FGF4 and FGFBP1
126 secretion by TNERT (Fig. 3G, H, Fig. S3C, D). Collectively the data shows that
127 increased NANOG enhances FGFR2 on the cell surface, and secretion of FGF4 and
128 FGFBP1 to intensify the FGF autocrine signaling. NANOG induces and enhances FGF
129 autocrine signaling through FGFR2 to execute *Nanog* autoregulation.

130

131 ***Nanog* autoregulation is a cell non-autonomous process mediated by FGF**
132 **autocrine/paracrine signaling.**

133

134 *Nanog* autorepression is suggested to operate by a cell-autonomous process
135 through intracellular proteins NANOG, ZFP281, and NURD complex(13). Cell non-
136 autonomous function of *Nanog* in the induction of primitive endoderm(33, 34) and
137 essentiality of secreted proteins FGF4 and FGFBP1 in autoregulation prompted us to
138 investigate cell non-autonomous mechanisms. We assessed the ability of conditioned
139 media from OHT induced TNERT cells, to repress *Nanog*:GFP in Tβc44Cre6 lacking

140 *Nanog* (Fig. 3I). The conditioned media was sufficient to repress the *Nanog*:GFP (Fig.
141 3J, Fig. S3E), suggesting that autoregulation operates via cell non-autonomous
142 mechanisms and discounts the direct role of NANOG in autoregulation as proposed
143 earlier(13). NANOG seems to be essential for triggering autoregulation through FGF
144 autocrine signaling but does not participate in repression. Further, the repression of
145 *Nanog:*GFP in TNERTZfp281-/- cell line lacking Zfp281 (Fig. S3F) suggests that
146 ZFP281 is dispensable for *Nanog* autoregulation (Fig. 3K).
147 To evaluate if FGF4 secretion was the causative factor of *Nanog* autoregulation
148 in the conditioned media, we treated Tβc44Cre6 with conditioned media from cells with
149 loss or gain of FGF4. The conditioned media from an E14Tg2a cell line overexpressing
150 FGF4 or supplementation of FGF4 (50ng/ml) could repress *Nanog*:GFP. Conversely, the
151 conditioned media from OHT induced TNERTFgf4-/- cells failed to repress *Nanog*:GFP,
152 suggesting FGF4 is the key secreted factor essential for *Nanog* autoregulation (Fig. 3L,
153 Fig. S3G). The ELISA analysis confirmed the secretion and accumulation of FGF4 and
154 FGFBP1 in the conditioned media (Fig. S3H-K). Collectively, our data establish that
155 *Nanog* autoregulation is a cell non-autonomous process triggered by NANOG by
156 augmenting FGF autocrine signaling.
157
158 **NANOG induced FGFR2 triggers autoregulation predominately in the ES cell**
159 **population with higher *Nanog* expression.**
160
161 *Nanog* autoregulation was proposed to restrict NANOG levels within limits to
162 retain the differentiation potential(13, 16). Autoregulation is expected to operate only in
163 *Nanog*-high cells in a population. To evaluate this logic, we used TDiN cell lines with
164 different induction levels of FaNANOG (Fig. S4A). The strength of *Nanog*
165 autoregulation was found to be dependent on the FaNANOG levels and was completely
166 abolished in TDiN clones with low FaNANOG (Fig. S4B, C). Further, the *Nanog:*GFP
167 was repressed only in 10% population of the TNERT with the highest *Nanog* expression
168 but not in the lowest 10% (Fig. 4A). Our experiments conclude that *Nanog*
169 autoregulation predominately operates in a subpopulation of cells with higher *Nanog*.
170 FGF4 and FGFBP1 are secreted proteins, hence cannot distinguish between the
171 *Nanog*-high and low cells in culture. Whereas FGFRs are essential for autoregulation
172 and are retained on the cells, we asked if FGFRs distinguish *Nanog*-high cells from low
173 cells in a population. We analyzed the correlation between the expression of FGFR1,
174 FGFR2, and NANOG in E14Tg2a by FACS. FGFR2 and FGFR1 showed a strong

175 correlation with NANOG, which was further enhanced for FGFR2-NANOG in SLPD
176 (r=0.80) whereas decreased for FGFR1-NANOG (r=0.59) in SLPD (Fig. 4B,) where
177 NANOG levels are higher. These data suggested FGFR2 but not FGFR1 expression
178 levels correlate and respond to NANOG concentration in the cells. FACS analysis
179 showed high FGFR2 in the 10% NANOG high population and lower FGFR2 in the 10%
180 NANOG low population (Fig. 4C). We analyzed the NANOG binding sequences in the
181 *Fgfr2* locus. Two NANOG binding regions (NBR) with multiple NANOG binding
182 sequences were identified in the *Fgfr2* locus from the ChIP-seq(28), NBR1 at 1.4 kb,
183 and NBR2 at -0.2 kb relative to TSS of *Fgfr2*. NBR1 and NBR2 were deleted in TNERT
184 (Fig. 4D, E, Fig. S4D, E). Autoregulation was operational in TNERTNBR1-/- albeit at
185 reduced strength, whereas it was abolished in TNERTNBR2-/- (Fig. 4F), suggesting that
186 NBR2 is essential for the binding of NANOG and activation of *Fgfr2* to trigger
187 autoregulation. Together, our data suggest dose-responsive induction of *Fgf4*, *Fgfbp1*,
188 and *Fgfr2* by NANOG. The *Nanog*-high cells secrete more FGF4 and FGFBP1, also
189 express higher FGFR2 receptors. The FGF4 in presence of FGFBP1 binds to FGFR2 to
190 enhance FGF signaling in *Nanog*-high cells to enhance pERK1/2 and repress *Nanog*. The
191 *Nanog*-low cells express relatively low FGFR2, resulting in weak FGF signaling and the
192 absence of autoregulation (Fig. 4G). We propose that FGFR2 distinguish the *Nanog*-high
193 cells from the low cells to activate ERK-driven autoregulation selectively in *Nanog*-high
194 cells.
195
196 **ERK1/2 interacts and recruits NONO to repress *Nanog* transcription.**
197
198 FGF signaling represses *Nanog* transcription(18, 35) and regulates *Nanog*
199 heterogeneity and monoallelic expression(12, 36, 37). How FGF signaling downstream
200 kinases repress *Nanog* is unclear. ERK can induce Tcf15 to repress *Nanog*(38) or it can
201 interact with NONO to regulate bivalent genes(39). We deleted *Tcf15* and *Nono* in
202 TNERT to generate TNERTTcf15-/- and TNERTNono-/- cell lines to examine their
203 function in autoregulation (Fig. 5A, Fig. S5A, B). OHT treatment failed to repress
204 *Nanog*:GFP in TNERTNono-/-, unlike in TNERTTcf15-/- indicating an essential role of
205 NONO but not TCF15 (Fig. 5B, Fig. S5A, C). NONO has been shown to activate
206 ERK1/2(39), and pERK1/2 was substantially reduced in TNERTNono-/- despite OHT
207 induction, unlike in TNERT (Fig. 5C, Fig. S5D). Endogenous immunoprecipitation
208 showed an interaction between NONO and ERK1/2, the interaction was maintained in
209 the presence or absence of NANOG (Fig. 5D). NONO colocalizes with ERK1/2 to

210 bivalent developmental genes to maintain poised POL2(39). The ChIP-seq data analysis
211 from Ma et. al.,(39) and Tee et. al.,(40) showed NONO and ERK1/2 occupancy on the
212 *Nanog* (Fig. S5E). We induced or repressed the pERK1/2 by treatment of E14Tg2a cells
213 with FGF4 or PD (Fig. 5E) and analyzed the occupancy of NONO, pERK1/2, POL2,
214 H3K4me3, and H3K27me3. The transcription start site (TSS) and 5 kb upstream region
215 (-5kb) are the two hubs of transcription factor binding and control of *Nanog*
216 transcription(41, 42). We performed ChiP-qPCR analysis with multiple primer sets
217 spanning the -5.8 kb to +1.5 kb region relative to TSS (Fig. 5F). pERK1/2 and NONO
218 binding was detected in immediate downstream regions of the -5kb, and TSS. Their
219 binding was reduced significantly in PD and enhanced in FGF4 suggesting pERK1/2 and
220 NONO binding on *Nanog* is dependent on FGF signaling (Fig. 5G, H). pERK1/2 was
221 shown to recruit NONO to bivalent genes(39). Although *Nanog* is not a bivalent gene,
222 our data suggests pERK1/2 recruits NONO to *Nanog*. POL2 occupancy seen in TSS and
223 downstream region was reduced in FGF4 and enhanced in PD treatment suggesting
224 active transcription of *Nanog* in PD and repression in FGF4 (Fig. 5I). This was
225 corroborated with enhanced enrichment of the transcription activating histone mark
226 H3K4me3 in PD (Fig. 5J) and enrichment of transcription repressive mark H3K27me3
227 at the -5kb region of the *Nanog* in FGF4 treatment (Fig. 5K). pERK1/2 phosphorylates
228 NANOG, USP21 and affects NANOG stability and transactivation capability(19, 43,
229 44). In agreement with NANOG destabilization by pERK1/2(19, 43, 45), The half-life
230 of NANOG was significantly compromised in FGF4 treated cells but enhanced in PD
231 (Fig. 5L, Fig. S5F), suggesting that the FGF/ERK represses *Nanog* transcription and also
232 affects NANOG stability. Collectively, these data suggest that FGF signaling activates
233 pERK1/2 and its binding onto *Nanog* in a concentration-dependent manner. pERK1/2 is
234 essential for the recruitment of NONO to the *Nanog* locus. pERK1/2-NONO are known
235 to poise the POL2 in bivalent genes(39). In contrast, pERK1/2-NONO affects POL2
236 loading onto the *Nanog* locus preventing the initiation of transcription. In the absence of
237 active FGF signaling, pERK1/2-NONO occupancy on the *Nanog* is decreased permitting
238 increased POL2 loading and transcription activation of the *Nanog* (Fig. 5M).
239
240 **NANOG regulates ERK signaling dynamics and heterogeneity**
241
242 ERK signaling regulates *Nanog* expression and heterogeneity in ES cells. Recently
243 pERK1/2 expression is reported to be heterogeneous and dynamic in ES cells and the
244 preimplantation embryos(24, 25, 46). We have shown that FGFR2 exhibits a negatively

245 skewed bimodal expression similar to *Nanog* in ESCs (Fig. 3F) and *Fgfr2* is induced in a
246 dosage-dependent manner by NANOG. We asked if NANOG dynamics could regulate
247 ERK signaling dynamics in ES cells through *Fgfr2*. Immunostaining showed
248 heterogeneous expression of NANOG and pERK1/2 in WT ESCs (E14Tg2a) with some
249 cells co-expressing both (Fig. 6A). Their expression showed a strong correlation
250 (r=0.6675) suggesting a positive association between NANOG and pERK1/2; similar to
251 NANOG and FGFR2. NANOG showed a broad range of expression as represented by the
252 broad range of relative fluorescence intensity (RFI 0-20000), pERK1/2 showed a
253 relatively narrow range of expression (RFI 1500-3000) in ESCs (Fig. 6B). The pERK1/2
254 expression in *Nanog* null ESC (TBC44Cre6) was very low relative to WT ESCs (RFI
255 <2000), suggesting pERK1/2 levels are dependent on NANOG. NANOG overexpression
256 in WT ESCs (EDiN) enhanced pERK1/2 levels by multiple folds relative to WT and
257 broadened the range of pERK1/2 levels (RFI >30000) (Fig. 6A) with a moderate
258 correlation between NANOG and pERK1/2 (r = 0.5375) (Fig. 6B). Intriguingly, high
259 levels of pERK1/2 failed to repress *Nanog* transgene and significantly reduce NANOG in
260 EDiN. This resulted in the coexistence of high pERK1/2 and high NANOG in the cells.
261 Despite very high levels of pERK1/2, *Nanog* over-expressing EDiN does not differentiate
262 suggesting that the *Nanog* function in ESC self-renewal is dominant over the pERK1/2
263 function in the differentiation of ESCs. These data suggest that pERK1/2 expression levels
264 and dynamic range of expression in ESCs are dependent on the expression level of *Nanog*
265 and its dynamics. To further validate this, we isolated *Nanog*-high subpopulation cells by
266 sorting the highest 10% iRFP expressing NiRPF2A reporter ESCs by FACS. The
267 expression of pERK1/2 and NANOG was analyzed in these cells every 4 hours during
268 their culture to study the dynamics of NANOG and pERK expression. The sorted cells
269 expressed NANOG and pERK1/2. After 4 hours of culture in fresh media, the NANOG
270 expression increased with a concomitant decrease in pERK1/2 (NANOG high-pERK1/2
271 low state). After 8 hours, the NANOG expression decreased and the pERK1/2 expression
272 increased. At 12 hrs the cells showed relatively low pERK1/2 and low NANOG
273 expression (Fig. 6C). A relative median fluorescence intensity plot of NANOG and
274 pERK1/2 suggests that NANOG and pERK1/2 follow a dynamic cycle of expression
275 during culture (Fig. 6D). This was further confirmed by immunostaining and imaging of
276 the sorted cell line at every 4 hr intervals (Fig. S6A). These results suggest that ESCs
277 continuously transit between different states of NANOG and pERK1/2 expression
278 resulting in heterogeneous and dynamic expression pERK1/2.
279

## Discussion

We demonstrate that the highest possible expression of *Nanog* could be achieved in SLPD by attaining a consistent low MEK1/2 activity. Wnt signaling can activate MEK1/2 at multiple levels(21), a relatively lower level of *Nanog* expression in SL2i and 2iL could be attributed to a time-dependent increase in MEK1/2 activity in presence of PD and CHIR (Fig. 1F, G). The inhibition of MEK1/2 prevents differentiation in 2iL, but a time-dependent increase in MEK1/2 activity is significant and sufficient to facilitate *Nanog* autoregulation. A time-dependent variation in MEK1/2 activity in 2iL opens up the plausibility of other molecular processes regulated by MEK1/2 activity to be functional in a naïve state.

Overexpression of *Nanog* is limited by an autorepression mechanism operating at the transcriptional level to retain the differentiation potential of ESCs(13, 16). Among the multiple possible pathways that can regulate *Nanog(17, 35, 38, 44)*, we show that FGF autocrine signaling is recruited for *Nanog* autoregulation. We show that a NANOG dosage-dependent differential induction of *Fgfr2* in *Nanog*-high ESCs triggers autoregulation by activation of ERK1/2. pERK1/2 recruits NONO to the *Nanog* locus and affects the loading of POL2 onto the *Nanog* locus reducing *Nanog* transcription (Fig. 5M). Other reports(19, 43) and our data show that pERK1/2 can affect NANOG stability and may contribute to autorepression. However, the inability of pERK1/2 to significantly repress NANOG expressed from a transgene and a strong correlation between NANOG-pERK1/2 (Fig. 6A, B) dismisses the possibility of significant contribution from post-transcriptional mechanisms in autoregulation. Our data suggest that *Nanog* autoregulation is triggered above a threshold of NANOG, thereafter the intensity of repression is dependent on the level of NANOG in the cell.

We show that NANOG activates ERK signaling by inducing *Fgfr2*, *Fgf4*, and *Fgfbp1.* The activated ERK1/2 together with NONO represses transcription of *Nanog,* resulting in a NANOG-pERK1/2 reciprocal regulatory loop (Fig. 6E). The subpopulation of ES cells expressing high NANOG will have higher FGFR2. This induces high ERK activity resulting in a high-NANOG:high-pERK state. The repression of *Nanog* transcription by pERK in these cells reduces NANOG, reducing transcription of *Fgfr2*. The cells traverse through various intermediate levels of NANOG and pERK1/2 resulting in a low-NANOG:low-pERK state. Low pERK1/2 permits activation of NANOG by other pluripotency factors gradually increasing NANOG in these cells. The increased NANOG activates *Fgfr2*, *Fgfbp1,* and *Fgf4* to induce ERK activity leading to

various intermediate levels of NANOG and pERK culminating in high-NANOG:high-pERK state. This induces a self-perpetuating cycle of activation of ERK signaling by NANOG and repression of *Nanog* by pERK1/2 leading to dynamic expression levels of NANOG and pERK1/2 in the ESC population (Fig. 6F).

pERK1/2 heterogeneity is suggested to be a vital determinant of fate choice in ICM and ES cells(24, 25, 45, 47, 48). The mechanism generating pERK1/2 heterogeneity is unclear. pERK1/2 heterogeneity may originate due to differential local concentrations of FGF4 or FGFBP1 or heterogeneous expression of receptors FGFRs or by negative feedback regulators (ETV5, DUSP1/6). *Nanog* is considered to induce FGF paracrine signaling through FGF4 secretion and specify primitive endoderm by cell-autonomous mechanisms(33, 34). Although FGF4 is essential for *Nanog* autoregulation, it is a secreted protein. Its induction by NANOG can neither explain the functioning of autoregulation exclusively in *Nanog*-high cells nor the heterogenous pERK1/2 activation in ESCs or ICM. FGFR1 is unlikely to induce ERK1/2 heterogeneity as it is relatively uniformly expressed in the epiblast(24, 25) and ESCs. Dosage-dependent induction of *Fgfr2* by NANOG and its accumulation on the surface of NANOG high cells can potentiate the cells to differentially respond to FGF4. Our data establish that the dosage-dependent induction of *Fgfr2* is the basis for differential activation of ERK1/2 in subpopulations of ESCs resulting in pERK1/2 heterogeneity. The carrier protein FGFBP1 may also locally enhance FGF signaling further contributing to pERK1/2 heterogeneity similar to heparan sulfate proteoglycans(49).

We propose the reciprocal regulation of *Nanog* by ERK signaling and ERK signaling by NANOG as the basis for both NANOG and pERK1/2 heterogeneity. We suggest that the NANOG-pERK axis may not merely be viewed as a mechanism of regulation of *Nanog* expression by ERK signaling, rather as a cyclic circuit where *Nanog* heterogeneity and expression dynamics lead to ERK signaling dynamics and vice versa. *Nanog* and ERK signaling are induced in multiple cancers(50, 51). The significance of the NANOG-pERK1/2 reciprocal regulatory loop in establishing heterogeneity and ERK signaling dynamics may not be limited to pluripotent cells but could be relevant in cancer stem cells and tumor heterogeneity.

**Acknowledgments**

HTK was supported by a fellowship from ICMR (India), DJ, VVV, MS was supported by a fellowship from UGC (India). RSR was supported by DBT grant No: BT/PR14064/GET/119/16/2015. PCS was supported by WT/DBT IA grant No:

500053/Z/09/Z. We thank the Microscopy, and FACS core facilities of CCMB for the support extended to carry out this work. We thank Ian chambers for his constructive comments on the manuscript.

**Author contributions**

Conceptualization, H.T.K, and P.C.S Methodology, H.T.K and P.C.S; Investigation, H.T.K, R.S.R., V.V.V., and G.S.; Writing – Original Draft, H.T.K. and P.C.S.; Writing – Review & Editing, H.T.K., and P.C.S.; Funding Acquisition, P.C.S.; Resources, H.T.K, R.S.R., M.S., and D.J.; Visualization, H.T.K, and D.J.; Supervision, P.C.S.

**Competing interest**

The authors declare no competing interests.

**Figure legends:**

**Fig. 1. Residual MEK1/2 activity in the ground state prevents complete derepression of *Nanog*.** (A) (left) FACS profiles of TβC44Cre6 cultured in indicated conditions for 3 passages. TβC44Cre6 is a *Nanog* null cell line, where *β–geo* cassette is inserted into one allele and GFP into another allele of the *Nanog* gene. The cells were cultured in Serum+LIF (SL) in presence of the 1 $\mu$M MEK1/2 inhibitor -PD0325901 (SLPD) or 3 $\mu$M GSK3$\beta$ inhibitor -CHIR99021 (SLCHIR) or in serum-free media - N2B27 with PD0325901, CHIR99021, and LIF (2iL). (right) *Nanog*:GFP population median of TβC44Cre6 (n=3). (B) (Left) FACS profile of NANOG-iRFP protein in NiRFP2A cells cultured in indicated conditions for 3 passages. (right) *NANOG*-iRFP population median of NiRFP2A (n=4). (C) RT-qPCR of pluripotency factors in indicated conditions (SL2i= SL+ PD0325901+CHIR99021). (D) RT-qPCR analysis of pre- mRNA of *Nanog* and *Oct4*. (E) (left)Western blot of NANOG, OCT4, and SOX2. (right) Relative NANOG levels as estimated by densitometry (n=8). NANOG was nearly 7-fold more in PD, which is twice that of 2iL/SL2i. (F) Western blot of pERK1/2 and ERK1/2 at 0, 1, 4, 8, 12, 16, and 24 hrs after media change in indicated treatments. (G) Western blot of pERK1/2 and ERK1/2 in SLPD, SLCHIR, 2iL, and SL2i after 8, 12, 16, and 24 hrs of culture relative to SL, where the cells in SL were harvested 24 hrs after the media change. (H) (left)Western blot of pERK1/2 and ERK1/2 in 1μM PD and increasing concentrations of CHIR in serum-free N2B27 media. (right) Relative pERK1/2 levels (n=3). (I)

385 (left)Western blot of pERK1/2 and ERK1/2 in 3μM CHIR and increasing concentrations
386 of PD in serum-free N2B27 media. (right) Relative pERK1/2 levels (n=6). All error bars
387 in the figure represent s.e.m.
388
389 **Fig. 2. FGF autocrine signaling pathway components are essential for *Nanog***
390 **autoregulation.** (A) (left) Schematic depiction of Tamoxifen (OHT) inducible TNERT
391 cell line. TNERT and TDiN (Fig. S2A, B) are similar to NERTc3 and 44iN(16), where
392 the NANOG function is reinstated by 4-Hydroxytamoxifen (OHT) or Doxycycline
393 respectively, and endogenous *Nanog* gene activity is reported by GFP. (Middle) FACS
394 profile of TNERT treated with OHT (red) or no OHT (blue). (Right) *Nanog*:GFP
395 population median of TNERT (n=3). (B) FACS profiles of TNERT, and TDiN treated
396 with 2$\mu$M SU5402, with OHT/Doxycycline (red) or no OHT/Doxycycline (blue). (C)
397 Heat map representing transcript levels (FPKM) of *Fgfbp1* from 8-cell to blastocyst stage
398 analyzed from the single-cell sequencing data. (D) Schematic depiction of TNERTFgfr1-
399 /-, TNERTFgfr2-/, TNERTFgf4-/-, and TNERTFgfbp1-/- cell lines, which are
400 derivatives of TNERT where *Fgfr1*, *Fgfr2*, *Fgf4,* and *Fgfbp1* are knocked out
401 respectively. (E) FACS profiles of TNERT, TNERTFgfr1-/-, TNERTFgfr2-/-,
402 TNERTFgf4-/-, and TNERTFgfbp1-/- cells, treated with OHT (red) or no OHT (blue).
403 All error bars in the figure represent s.e.m.
404
405 **Fig. 3. NANOG triggers autoregulation by inducing the expression of FGFR2,**
406 **FGF4, and FGFBP1.**
407 (A) RT-qPCR showing relative transcript levels after 0, 0.5, 1, 2, 4, 8, 12 and 18 hrs
408 OHT treatment in TNERT (n=3). *Esrrb,* a known direct target of NANOG was used as
409 positive control. (B) RT-qPCR of relative levels of pre- mRNA at the above indicated
410 time points after OHT treatment in TNERT (n=3). (C) ChIP analysis of NANOG on
411 *Fgf4*, *Fgfbp1*, *Fgfr1*, *Fgfr2,* and *Nanog* genes in E14Tg2a cells cultured in SL or SLPD
412 for 48 hrs (n=4). (D) ChIP analysis of NANOG on promoters of above-indicated loci in
413 EDiN cells cultured in Doxycycline (red) or no Doxycycline (blue) for 48 hrs (n=3). (E)
414 Western blot of FGFR1, FGFR2, and pERK1/2 in TNERT after 18 hrs treatment with or
415 no OHT. (F) FACS analysis of FGFR2 on the cell surface of TNERT treated with (red)
416 or no OHT (blue) (n=3). (G-H) ELISA-based relative quantification of FGF4 (G) and
417 FGFBP1 (H) in conditioned media from TNERT treated with or no OHT (n=3). (I)
418 Schematic of conditioned media experiment. (J) FACS analysis of Tβc44Cre6 cell line

419 in conditioned media collected from TNERT treated with OHT after 0, 18, 24, and 48
420 hrs. (K) (left) FACS analysis of TNERTZfp281-/- cells treated with (red) or with no
421 OHT (blue) treatment. (right) *Nanog*:GFP population median of TNERTZfp281-/-
422 (n=3). (L) FACS analysis of Tβc44Cre6 cell line in conditioned media from,
423 TNERT+OHT 0 hrs, TNERTFGF4-/-, Tβc44Cre6 48 hrs, E14Tg2a- FGF4-OE
424 (overexpression) 48 hrs, TNERT+OHT 48 hrs and 50ng/ml FGF4. All error bars in the
425 figure represent s.e.m.
426
427 **Fig. 4. NANOG induced FGFR2 triggers autoregulation predominately in the ES**
428 **cell population with higher *Nanog* expression.** (A) (top) To analyze autoregulation in
429 *Nanog*-high and *Nanog*-low cells, we sorted the lowest and the highest 10% population
430 of the TNERT expressing GFP and treated with OHT. FACS profile of TNERT, the
431 position of the gates indicates the 10% low-*Nanog*:GFP (LN) and 10% high-*Nanog*:GFP
432 (HN) population sorted for culture. (Bottom left) FACS profiles of LN and HN after 18
433 hrs culture in SL. LN (dark green), HN (dark maroon) in SL, and LN (light green), HN
434 (light maroon) in SL+ OHT. (Bottom right) *Nanog*:GFP population median of TNERT
435 (n=3). (B) FACS profile of E14Tg2a cultured in SL or SLPD for 48 hrs and co-
436 immunostained with anti-NANOG and anti-FGFR1 or anti-FGFR2 antibodies. r-values
437 represent the average of 3 independent experiments (n=3). (C) (left) FACS profile of
438 E14Tg2a immunostained with anti-NANOG and anti-FGFR2 antibody, the gates mark
439 the 10% low-NANOG (LN) and 10% high-NANOG (HN) population. (right) Histogram
440 depicting the FGFR2 expression profiles in the gated LN and HN cell population (n=3).
441 (D-E) Schematic representation of TNERTNBR1-/- (D) and TNERTNBR2-/- (E) cells,
442 in which NANOG binding sequences at +1.4 kb (NBR1) and -0.2 kb (NBR2) are deleted
443 respectively. (F) (Top) FACS profiles of TNERT, TNERTNBR1-/-, and TNERTNBR2-
444 /- with (red) or no OHT treatment (blue). (bottom) *Nanog*:GFP population median of
445 TNERT, TNERTNBR1-/- and TNERTNBR2-/- with or no OHT treatment. (G) A
446 cartoon depicting *Nanog* autoregulation in *Nanog*-high cells. The *Nanog*-high cells
447 secrete more FGF4 and FGFBP1. They contain higher levels of FGFR2 on the surface
448 and are hence more sensitive to the FGF ligand triggering a stronger FGF signaling. The
449 increased pERK1/2 in these cells recruit NONO to the *Nanog* locus and represses *Nanog*
450 transcription. The *Nanog*-low cells secrete very little FGF4 and FGFBP1 and present
451 fewer FGFR2 on their surface and are less sensitive to FGF signaling. The pERK1/2
452 levels in *Nanog*-low cells are insufficient to execute *Nanog* autoregulation. All error bars
453 in the figure represent s.e.m.

454

455 **Fig. 5. ERK1/2 interacts and recruits NONO to repress *Nanog* transcription.** (A)
456 Schematic of TNERTNono-/-cell line; a derivative of TNERT in which *Nono* is
457 knocked-out. (B) FACS profile of TNERTNono-/- treated with or no OHT (n=3). (C)
458 Western blot of pERK1/2 and ERK1/2 in TNERT and TNERTNono-/- cells treated with
459 or no OHT (n=3). (D) Immunoprecipitation analysis showing interactions between
460 ERK1/2 and NONO in the presence or absence of *Nanog* induction by Doxycycline in
461 TDiN cells. (E) (left) Western blot of pERK1/2 and ERK1/2 in E14Tg2a cells treated
462 with PD or FGF4. (right) Relative levels of pERK1/2 in E14Tg2a cells treated with PD
463 or FGF4 (n=4). (F) Schematic representation of *Nanog* locus comprising the -6.0 to +2kb
464 region. The vertical bars represent relative positions of primer pairs used for ChiP-qPCR
465 analysis. S1-S6 are located upstream of the TSS, S7 primer pair is located around TSS,
466 S8 and S9 are located downstream in the first intron. (G-K) ChIP-qPCR analysis of
467 pERK1/2 (G), NONO (H), Pol2 (I), H3K4me3 (J) and H3K27me3 (K) on *Nanog* 5'
468 region in E14Tg2a cells (blue), treated with FGF4 (green) and with PD (pink) (n=3). (L)
469 Cycloheximide chase assay of NANOG in SL, SLPD, and SLFGF4 in E14Tg2a cells.
470 (M) A cartoon illustrating the repression of *Nanog* by FGF signaling and derepression
471 of *Nanog* in absence of FGF signaling. The FGF4 activates the FGF signaling cascade,
472 resulting in phosphorylation of ERK1/2. pERK1/2 interacts and recruits NONO to the
473 *Nanog* promoter and represses transcription of *Nanog*. pERK1/2 also affects the stability
474 of the NANOG. In absence of FGF4, the pERK1/2 levels decrease resulting in enhanced
475 stability of NANOG and transcription of *Nanog* locus by NANOG and other
476 pluripotency factors resulting in derepression of *Nanog* locus. All error bars represent
477 s.e.m.

478

479 **Fig. 6. NANOG regulates ERK signaling dynamics and heterogeneity**
480 (A) Immunofluorescence of pERK1/2 (red) and NANOG (green) in the indicated ESCs.
481 (B)The normalized fluorescence intensity of pERK1/2 was plotted against the
482 normalized fluorescent intensity of NANOG. (C) Contour plot of FACS analysis of
483 pERK1/2 and NANOG in 10% NANOG-high NiRFP2A cells cultured for the indicated
484 time. (D) A plot of median fluorescence intensity of pERK1/2 and NANOG relative to
485 0 hrs culture of 10% NANOG-high NiRFP2A cells. The NANOG and pERK1/2
486 expression oscillate between high and low levels in the cells during the course of culture.
487 (E) A working model of the NANOG-pERK1/2 reciprocal regulatory loop operating in
488 ESCs. NANOG induces *Fgfbp1* and *Fgfr2 to* enhance ERK signaling in *Nanog*-high

489 cells. pERK1/2 along with NONO occupy the *Nanog* promoter to repress its
490 transcription. The transcription repression results in reduced NANOG, which prevents
491 induction of *Fgfbp1*and *Fgfr2.* The is reduces ERK activity relieving the repression on
492 the *Nanog* promoter. (F) A schematic depicting the progression of cells through different
493 expression states of NANOG and pERK1/2 expression in the ESC population. The cells
494 expressing high-NANOG induce *Fgfbp1* and *Fgfr2* to activate pERK by autocrine
495 signaling to give rise to a high-NANOG:high-pERK state. The repression of *Nanog*
496 transcription by pERK leads the cells through different intermediate levels of expression
497 of NANOG and pERK resulting in a low-NANOG:low-pERK state. The low pERK
498 permits transcription of *Nanog* and gradual induction of *Fgfbp1* and *Fgfr2* by NANOG
499 culminating in a high-NANOG:high-pERK state. The cells will cycle through different
500 levels of pERK and NANOG levels generating a heterogeneous population with a strong
501 correlation between pERK and NANOG in an ESC cells culture.
502
503 **Methods:**
504 **Cell Culture:** The cell lines used in this study and their origin is depicted in Fig. S7. All
505 the cells used in this study are derivatives of E14Tg2a ES. The cells were cultured as
506 described earlier (2). 4-Hydroxytamoxifen (4-OHT), Doxycycline, and Cycloheximide
507 were used at a concentration of 1 μg/ml, 1 μg/ml, and 100 μg/ml respectively. The TNERT
508 and its derivative cell lines were treated with 4-OHT for 18 hrs except when indicated.
509 TDiN and EDiN were treated with Doxycycline for 48 hrs unless indicated. CHIR99021
510 (CHIR, PD0325901 (PD), and SU5402 were used at 3 μM, 1 μM, and 2 μM, respectively,
511 except when indicated. FGF4 and FGFBP1 were used at 50ng/ml concentration. The cells
512 were cultured in Serum+ LIF (SL), SL+ PD (SLPD), SL+CHIR (SLCHIR), SL+SU5402
513 (SLSU5402), SL + PD +CHIR (SL2i) and N2B27+LIF+PD+CHIR (2iL) for at least 2
514 passages before treating with either 4-OHT or Doxycycline.
515 The cells were cultured on cell culture dishes coated with 0.1% gelatin for all
516 experiments. The conditioned media from the cells was collected after the specific
517 treatments or indicated time points. The conditioned media was passed through a 0.22
518 μM filter and added to Tβc44Cre6 or TNERT cells. The cells were cultured in the
519 conditioned media for 24 hrs before FACS analysis.
520
521 **Generation of Knock-out cell lines using paired CRISPR constructs:** pU6-iRFP
522 (pU6-Cas9-T2A-iRFP-2A-PuroR) construct was engineered by replacing mCherry

523 coding sequence with iRFP670-2A-PuroR cassette in pU6-(BbsI)-CBh-Cas9-T2A-
524 mCherry plasmid (Addgene 64324) by Gibson assembly. For generating knock-out of a
525 gene, two sgRNAs were designed with the expected cutting sites at least 30 bps apart to
526 achieve deletion of at least 30 bps or more. For genotyping of the deletions, a set of
527 genotyping primers was designed outside the deletion region flanking the sgRNA pair.
528 The sgRNAs were designed using the UCSC genome browser and Deskgen or
529 Benchling. The sequences of the sgRNAs and the genotyping primers are detailed in
530 Table S1. All sgRNAs were cloned into pU6-Cas9-T2A-iRFP-2A-PuroR plasmids. To
531 generate a paired sgRNA construct, the U6-SgRNA cassette from one plasmid
532 containing the sgRNA was amplified and Gibson assembled into the XbaI site of the
533 plasmid containing the other sgRNA pair of the pair. Around 1 µg of paired sgRNA
534 CRISPR plasmid was nucleofected in 1 million cells. The transfected cells were sorted
535 by FACS for iRFP expression and cultured to obtain clones. The clones were genotyped
536 by PCR using respective primer sets to identify the heterozygous and homozygous
537 clones. The sequence of the derivation of cell lines is described in Fig. S7.
538
539 **Generation of Knock-in cell lines**: A sgRNA encompassing the stop codon of *Nanog*
540 was cloned into pU6-iRFP and co-transfected with the targeting vectors. The 2A-mCherry
541 cassette was replaced with iRFP sequences by Gibson assembly in Nanog-2A-mCherry
542 targeting vector (Addgene 59995) to generate Nanog iRFP670 fusion targeting vector.
543 Around 3 µg plasmid (targeting vector and CRISPR plasmid) were nucleofected in 3
544 million E14Tg2a cells. The cells were selected against G418. The derivation of cell lines
545 is described in Fig. S7.
546
547 **Real-time PCR analysis:** The RNA was extracted with TRIZOL reagent and quantified
548 using a Nanodrop2000 spectrophotometer (Thermo Fisher Scientific). One microgram of
549 total RNA was reversed transcribed into cDNA by using superscript III. All real-time PCR
550 was carried out with Power SYBR Green PCR master mix on the ABI prism 7900 HT
551 sequence detection system (ABI) as per the manufacturer's instructions. GAPDH was
552 used as an internal control or normalizer. The data was analyzed by SDS 2.2 software
553 provided with the instrument. The primers used for real-time PCR are given in Table S1.
554
555 **Western blot analysis:** The cells were harvested by using RIPA buffer with 25mM Tris
556 HCl (pH 8.0), 150mM NaCl, 1%NP-40, 0.5% Sodium deoxycholate, 0.1% SDS and
557 Complete Protease Inhibitor Cocktail Tablets (Roche). The protein samples were

558 resolved by 4-20% gradient SDS-PAGE and electroblotted on to polyvinylidene
559 difluoride (PVDF) membrane. The blot was blocked with 3% Blotto for an hour and
560 incubated overnight with a primary antibody at 4ºC. Blots were washed thrice with TBST
561 and hybridized with secondary antibody and the blots were visualized using enhanced
562 chemiluminescence (ECL)detection kit. Western blot quantifications were performed
563 using Image lab (Bio-rad).
564
565 **Chromatin Immunoprecipitation (ChIP):** Cells were fixed by adding 270 µL of 37%
566 formaldehyde into 10 ml of media and incubated for 10 minutes at 37ºC to crosslink the
567 chromatin. Cells were washed twice with cold PBS containing protease inhibitors. Cells
568 were scraped and harvested by centrifugation. The cell pellet was dissolved in 200 µL of
569 SDS Lysis Buffer (1% SDS, 10 mM EDTA, and 50 mM Tris, pH 8.0) containing protease
570 inhibitors (per $10^6$ cells) and incubated on ice for 10 min. The 25 cycles of sonication
571 were used to shear DNA between 200 to1000 base pairs. The sample was centrifuged at
572 13,000 rpm for 10 min (at 4°C). The supernatant was diluted by adding 1800 µl ChIP
573 Dilution Buffer (1.1% Triton X- 100, 1.2 mM EDTA, 16.7 mM Tris-HCl, pH 8.0, 167
574 mM NaCl with protease inhibitors). The 1% input was aliquoted from the supernatant. To
575 reduce nonspecific background, diluted cell supernatant was preabsorbed for one hour at
576 4ºC with protein A/G magnetic beads (Invitrogen). The supernatant fraction was
577 incubated overnight at 4°C with an appropriate antibody and protein A/G magnetic beads
578 were blocked with 4% BSA, 2µg salmon sperm DNA. The next day, pre-blocked beads
579 were mixed with the sample and incubated for 1 hour to capture the antibodies. The
580 supernatant was discarded and washed in the given order with 1 mL of each of the buffers
581 - Low Salt Wash Buffer (0.1% SDS, 1% Triton X-100, 2 mM EDTA, 20 mM Tris-HCl,
582 pH 8.0, 150 mM NaCl), High Salt Wash Buffer (0.1% SDS, 1% Triton X-100, 2 mM
583 EDTA, 20 mM Tris-HCl, pH 8.0, 500 mM NaCl), LiCl Wash Buffer (0.25 M LiCl, 1%
584 IGEPAL-CA630, 1% deoxycholic acid, 1 mM EDTA, 10 mM Tris, pH 8.0.), and TE
585 buffer. DNA was eluted with elution buffer (1%SDS, 0.1M NaHCO3). The sample input
586 and the ChIP chromatin were reverse crosslinked with 20 µL of 5 M NaCl by heating at
587 65°C for 4 hours. Followed by one hour at 45°C with 10 µL of 0.5 M EDTA, 20 µL 1 M
588 Tris- HCl, pH 6.5, and 2 µL of 10 mg/mL Proteinase K. Finally, DNA was eluted in 50
589 µL water using a minEleute PCR purification kit. Then 1µL of sample and input was used
590 for qPCR analysis. The primers used for qPCR analysis were listed in Table S1.
591
592 **Co-Immunoprecipitation in ES cells:** 10-12 million ES cells were harvested by

593 trypsinization, washed twice with cold PBS, and resuspended in 800 µl of CoIP Lysis
594 Buffer (50 mM Tris-HCl, pH 67.5; 350 mM NaCl, 0.7% NP40, EDTA 0.1mM, 20%
595 (v/v) glycerol, and protease inhibitor cocktail). The cell lysate was mixed with protein
596 A/G magnetic beads for 1 hour at 4ºC for pre-clearing the background. Then 5% input
597 was aliquoted and the remaining supernatant was incubated overnight with appropriate
598 primary antibody. The protein A/G magnetic beads were blocked overnight at 4ºC with
599 200 µl of CoIP Lysis buffer containing 4% BSA. The next day, the beads were
600 transferred to the primary antibody incubated tubes and incubated for one hour at 4ºC.
601 The bead was washed three times with ice-cold TBS150 (50mM Tris, 150mM NaCl) and
602 the protein was eluted with 2X sample buffer (125 mM Tris-HCl, pH 6.8**,** 4% SDS**,** 20%
603 (v/v) glycerol, 0.004% bromophenol blue), by boiling for 5 min. The western was done
604 for sample and input and the interaction was analyzed.
605
606 **Immunocytochemistry:** The cells were cultured in 24 well dishes and fixed in 3.7%
607 formaldehyde diluted in PBS for 15 mins at RT. After 3 washes with PBS, the cells were
608 permeabilized and blocked with PBS containing 0.5% BSA and 0.3% Triton-X100 for 1
609 hour at room temperature. The cells were hybridized with primary antibody (1:100
610 dilution) in PBS containing 0.5% BSA at 4ºC overnight in a humidified chamber. The
611 cells were washed three times with PBS and hybridized to appropriate secondary
612 antibody at 1:1000 dilution room temperature for 1hour. The nuclei were stained with
613 DAPI in 1X PBS for 20 min at room temperature. The cells were washed thrice with
614 PBS. The cells were layered with 100 µl of the mixture of PBS and Glycerol (1:1) and
615 the images were acquired on the ZEISS Axio observer microscope and analyzed using
616 ImageJ software.
617
618 **ELISA Assay:** The condition media from the cell lines was collected at the respective
619 time points. 100 µl of the media was coated per well of 96 wells of ELISA plate by
620 incubating overnight at 4ºC. The wells were washed thrice with PBS containing 0.05%
621 Tween-20 and blocked with PBS containing 2% BSA for one hour at room temperature.
622 The wells were washed once with PBS and incubated with the appropriate primary
623 antibody (1:100) for one hour. Washed thrice with PBST, an appropriate HRP-labeled
624 secondary antibody was hybridized for one hour at room temperature. The wells were
625 washed thrice with PBST and incubated in substrate solution OPD (o-phenylenediamine
626 dihydrochloride) 3mg/ml with 6 µl/ml $H_2O_2$) for 30 min in dark. The reaction was stopped
627 by using 2N $H_2SO_4$. The absorbance was measured at 492 nm in Power wave XS2 (Bio

628 Tek instruments).

629

630 **FACS analysis:**

631 **Reporter cells:** Cells were trypsinized and collected by spinning at 800 rpm for 5 min.
632 The media was removed and cells were resuspended in 300 µl of PBS containing 2%
633 FBS at $10^6$ cells/ml. The samples were analyzed in the Gallios flow cytometer (Beckman
634 Coulter) or Fortessa flow cytometer (BD Biosciences). Sorting was performed on a
635 MoFlo-XDP cell sorter (Beckman Coulter).

636 **Immunostained cells**: Cells were harvested by treatment with 0.5 mM EDTA and
637 resuspended into single cells. The cells were fixed in PBS with 4% paraformaldehyde
638 (PFA) for 20 min at room temperature. Cells were washed twice with cold PBS and
639 incubated with methanol for 30 min for permeabilization. In the case of experiments
640 involving the analysis of FGFRs on the cell surface, the permeabilization step was
641 excluded. Then cells were blocked with PBS containing 0.5% BSA for 60 min at room
642 temperature. The cells were washed and hybridized to the appropriate primary antibody
643 at 4ºC overnight. The cells were washed thrice with PBS and hybridized to the
644 appropriate secondary antibody in PBS containing 0.5% BSA at1:1000 dilution for one
645 hour at room temperature. The cells were washed thrice with PBS and the fluorescence
646 profiles were acquired in the Gallios FACS analyzer (Beckman Coulter). All the FACS
647 data were analyzed using FlowJo software (BD Biosciences).

648

649 **Statistical analysis and reproducibility:** Statistical analysis was done by using a two-
650 tailed paired or unpaired student t-test. The representation of data is in the form of
651 means+/-SEM. The mean was calculated for more than three independent experiments *P*
652 value<0.05 is considered as statistically significant. * represents P<0.05, ** represents
653 P<0.001, *** represents P<0.0001, and **** represents P<0.00001.

654

655 **References**

656


657 1. I. Chambers *et al.*, Nanog safeguards pluripotency and mediates germline
658 development. **450**, 1230-1234 (2007).
659 2. N. Festuccia *et al.*, Esrrb is a direct Nanog target gene that can substitute for Nanog
660 function in pluripotent cells. **11**, 477-490 (2012).
661 3. A. Filipczyk *et al.*, Biallelic expression of nanog protein in mouse embryonic stem
662 cells. **13**, 12-13 (2013).
663 4. K. Hayashi, S. M. C. de Sousa Lopes, F. Tang, M. A. J. C. s. c. Surani, Dynamic
664 equilibrium and heterogeneity of mouse pluripotent stem cells with distinct

665 functional and epigenetic states. **3**, 391-401 (2008).
666 5. T. Kalmar *et al.*, Regulated fluctuations in nanog expression mediate cell fate
667 decisions in embryonic stem cells. **7**, e1000149 (2009).
668 6. H. Niwa, K. Ogawa, D. Shimosato, K. J. N. Adachi, A parallel circuit of LIF
669 signalling pathways maintains pluripotency of mouse ES cells. **460**, 118-122
670 (2009).
671 7. M.-E. Torres-Padilla, I. J. D. Chambers, Transcription factor heterogeneity in
672 pluripotent stem cells: a stochastic advantage. **141**, 2173-2181 (2014).
673 8. Y. Toyooka, D. Shimosato, K. Murakami, K. Takahashi, H. J. D. Niwa,
674 Identification and characterization of subpopulations in undifferentiated ES cell
675 culture. **135**, 909-918 (2008).
676 9. D. L. van den Berg *et al.*, Estrogen-related receptor beta interacts with Oct4 to
677 positively regulate Nanog gene expression. **28**, 5986-5995 (2008).
678 10. I. Chambers *et al.*, Functional expression cloning of Nanog, a pluripotency
679 sustaining factor in embryonic stem cells. **113**, 643-655 (2003).
680 11. K. Mitsui *et al.*, The homeoprotein Nanog is required for maintenance of
681 pluripotency in mouse epiblast and ES cells. **113**, 631-642 (2003).
682 12. Y. Miyanari, M.-E. J. N. Torres-Padilla, Control of ground-state pluripotency by
683 allelic regulation of Nanog. **483**, 470-473 (2012).
684 13. M. Fidalgo *et al.*, Zfp281 mediates Nanog autorepression through recruitment of
685 the NuRD complex and inhibits somatic cell reprogramming. **109**, 16202-16207
686 (2012).
687 14. M. Fidalgo *et al.*, Zfp281 functions as a transcriptional repressor for pluripotency
688 of mouse embryonic stem cells. **29**, 1705-1716 (2011).
689 15. S. Mora-Castilla *et al.*, Nitric oxide repression of Nanog promotes mouse
690 embryonic stem cell differentiation. **17**, 1025-1033 (2010).
691 16. P. Navarro *et al.*, OCT4/SOX2-independent Nanog autorepression modulates
692 heterogeneous Nanog gene expression in mouse ES cells. **31**, 4547-4562 (2012).
693 17. L. Pereira, F. Yi, B. J. J. M. Merrill, c. biology, Repression of Nanog gene
694 transcription by Tcf3 limits embryonic stem cell self-renewal. **26**, 7479-7491
695 (2006).
696 18. T. Hamazaki, S. M. Kehoe, T. Nakano, N. J. M. Terada, c. biology, The Grb2/Mek
697 pathway represses Nanog in murine embryonic stem cells. **26**, 7539-7549 (2006).
698 19. S.-H. Kim *et al.*, ERK1 phosphorylates Nanog to regulate protein stability and
699 stem cell self-renewal. **13**, 1-11 (2014).
700 20. D. A. Faddah *et al.*, Single-cell analysis reveals that expression of nanog is
701 biallelic and equally variable as that of other pluripotency factors in mouse ESCs.
702 **13**, 23-29 (2013).
703 21. M.-S. Yun, S.-E. Kim, S. H. Jeon, J.-S. Lee, K.-Y. J. J. o. c. s. Choi, Both ERK
704 and Wnt/β-catenin pathways are involved in Wnt3a-induced proliferation. **118**,
705 313-322 (2005).
706 22. T. Kunath *et al.*, FGF stimulation of the Erk1/2 signalling cascade triggers
707 transition of pluripotent embryonic stem cells from self-renewal to lineage
708 commitment. **134**, 2895-2902 (2007).
709 23. F. Lanner, J. J. D. Rossant, The role of FGF/Erk signaling in pluripotent cells. **137**,
710 3351-3360 (2010).
711 24. M. Kang, V. Garg, A.-K. J. D. c. Hadjantonakis, Lineage establishment and
712 progression within the inner cell mass of the mouse blastocyst requires FGFR1
713 and FGFR2. **41**, 496-510. e495 (2017).
714 25. A. Molotkov, P. Mazot, J. R. Brewer, R. M. Cinalli, P. J. D. c. Soriano, Distinct
715 requirements for FGFR1 and FGFR2 in primitive endoderm development and exit
716 from pluripotency. **41**, 511-526. e514 (2017).

717 26. S.-J. Park, K. Shirahige, M. Ohsugi, K. J. N. a. r. Nakai, DBTMEE: a database of
718 transcriptome in mouse early embryos. **43**, D771-D776 (2015).
719 27. E. Tassi *et al.*, Enhancement of fibroblast growth factor (FGF) activity by an FGF-
720 binding protein. **276**, 40247-40253 (2001).
721 28. V. Karwacki-Neisius *et al.*, Reduced Oct4 expression directs a robust pluripotent
722 state with distinct signaling activity and increased enhancer occupancy by Oct4
723 and Nanog. **12**, 531-545 (2013).
724 29. D. M. Ornitz *et al.*, Receptor specificity of the fibroblast growth factor family.
725 **271**, 15292-15297 (1996).
726 30. X. Zhang *et al.*, Receptor specificity of the fibroblast growth factor family: the
727 complete mammalian FGF family. **281**, 15694-15700 (2006).
728 31. G. Auciello, D. L. Cunningham, T. Tatar, J. K. Heath, J. Z. J. J. o. c. s. Rappoport,
729 Regulation of fibroblast growth factor receptor signalling and trafficking by Src
730 and Eps8. **126**, 613-624 (2013).
731 32. C. Francavilla *et al.*, Functional proteomics defines the molecular switch
732 underlying FGF receptor trafficking and cellular outputs. **51**, 707-722 (2013).
733 33. S. Frankenberg *et al.*, Primitive endoderm differentiates via a three-step
734 mechanism involving Nanog and RTK signaling. **21**, 1005-1013 (2011).
735 34. D. M. Messerschmidt, R. J. D. b. Kemler, Nanog is required for primitive
736 endoderm formation through a non-cell autonomous mechanism. **344**, 129-137
737 (2010).
738 35. K. E. Santostefano, T. Hamazaki, C. E. Pardo, M. P. Kladde, N. J. J. o. B. C.
739 Terada, Fibroblast growth factor receptor 2 homodimerization rapidly reduces
740 transcription of the pluripotency gene Nanog without dissociation of activating
741 transcription factors. **287**, 30507-30517 (2012).
742 36. J. Nichols, J. Silva, M. Roode, A. J. D. Smith, Suppression of Erk signalling
743 promotes ground state pluripotency in the mouse embryo. **136**, 3215-3222 (2009).
744 37. J. Wray, T. Kalkan, A. G. J. B. S. T. Smith, The ground state of pluripotency. **38**,
745 1027-1032 (2010).
746 38. O. R. Davies *et al.*, Tcf15 primes pluripotent cells for differentiation. *Cell reports*
747 **3**, 472-484 (2013).
748 39. C. Ma *et al.*, Nono, a bivalent domain factor, regulates Erk signaling and mouse
749 embryonic stem cell pluripotency. **17**, 997-1007 (2016).
750 40. W.-W. Tee, S. S. Shen, O. Oksuz, V. Narendra, D. J. C. Reinberg, Erk1/2 activity
751 promotes chromatin features and RNAPII phosphorylation at developmental
752 promoters in mouse ESCs. **156**, 678-690 (2014).
753 41. X. Chen *et al.*, Integration of external signaling pathways with the core
754 transcriptional network in embryonic stem cells. **133**, 1106-1117 (2008).
755 42. Y.-H. Loh *et al.*, The Oct4 and Nanog transcription network regulates pluripotency
756 in mouse embryonic stem cells. **38**, 431-440 (2006).
757 43. J. Brumbaugh *et al.*, NANOG is multiply phosphorylated and directly modified
758 by ERK2 and CDK1 in vitro. **2**, 18-25 (2014).
759 44. J. Jin *et al.*, The deubiquitinase USP21 maintains the stemness of mouse
760 embryonic stem cells via stabilization of Nanog. **7**, 1-15 (2016).
761 45. M. J. Pokrass *et al.*, Cell-cycle-dependent ERK signaling dynamics direct fate
762 specification in the mammalian preimplantation embryo. **55**, 328-340. e325
763 (2020).
764 46. J. Deathridge, V. Antolović, M. Parsons, J. R. Chubb, Live imaging of ERK
765 signalling dynamics in differentiating mouse embryonic stem cells. *Development*
766 **146**, dev172940 (2019).
767 47. S. Bessonnard *et al.*, Gata6, Nanog and Erk signaling control cell fate in the inner
768 cell mass through a tristable regulatory network. **141**, 3637-3648 (2014).

48. C. S. Simon, S. Rahman, D. Raina, C. Schröter, A.-K. J. D. C. Hadjantonakis, Live Visualization of ERK Activity in the Mouse Blastocyst Reveals Lineage-Specific Signaling Dynamics. **55**, 341-353. e345 (2020).
49. M. V. Galanternik, K. L. Kramer, T. J. C. r. Piotrowski, Heparan sulfate proteoglycans regulate Fgf signaling and cell polarity during collective cell migration. **10**, 414-428 (2015).
50. K. Song *et al.*, API5 confers cancer stem cell-like properties through the FGF2-NANOG axis. *Oncogenesis* **6**, e285-e285 (2017).
51. C. Huang *et al.*, ERK1/2-Nanog signaling pathway enhances CD44 (+) cancer stem-like cell phenotypes and epithelial-to-mesenchymal transition in head and neck squamous cell carcinomas. *Cell death & disease* **11**, 1-14 (2020).

## Figure 1

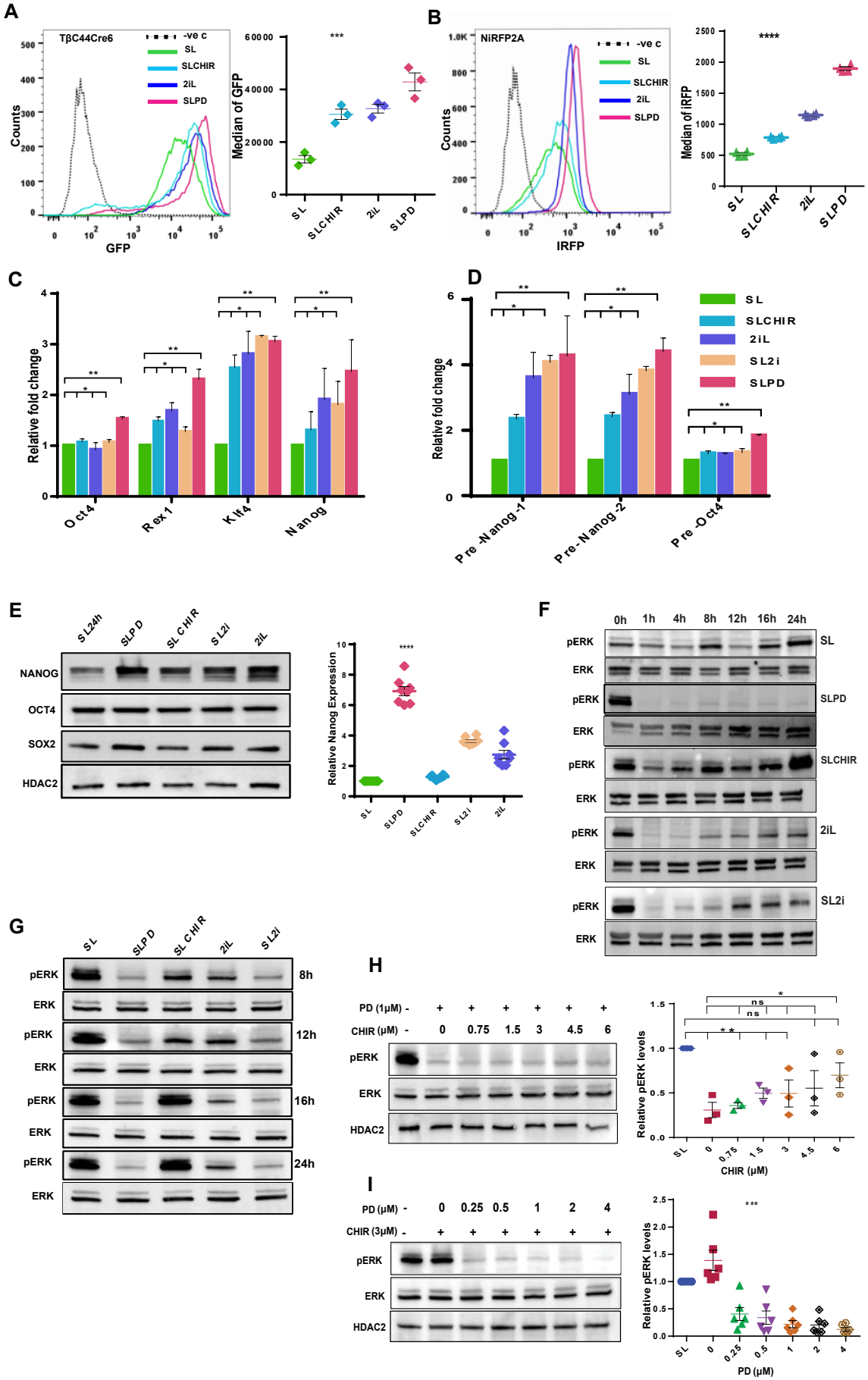
A
TβC44Cre6
-ve c
SL
SLCHIR
2iL
SLPD
Counts
GFP
Median of GFP
B
NiRFP2A
IRFP
Median of iRFP
C
Relative fold change
Oct4
Rex1
Klf4
Nanog
D
SL2i
Pre-Nanog-1
Pre-Nanog-2
Pre-Oct4
E
SL24h
NANOG
OCT4
SOX2
HDAC2
Relative Nanog Expression
F
0h
1h
4h
8h
12h
16h
24h
pERK
ERK
G
8h
12h
16h
24h
H
PD (1μM)
CHIR (μM)
Relative pERK levels
I
PD (μM)
CHIR (3μM)

## Figure 2

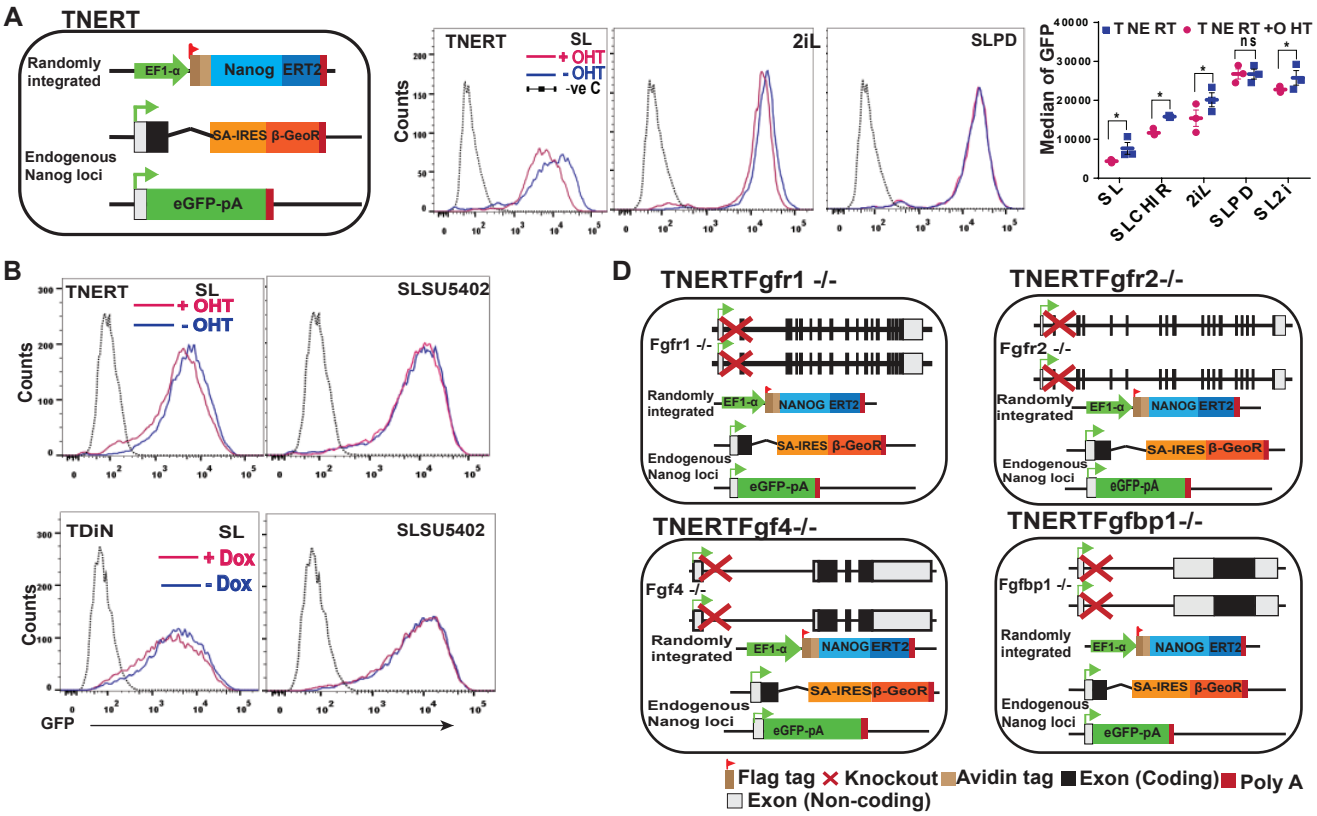
A
TNERT
Randomly integrated
EF1-α
Nanog
ERT2
SA-IRES
β-GeoR
Endogenous Nanog loci
eGFP-pA
TNERT
SL
+ OHT
- OHT
-ve C
2iL
SLPD
Counts
Median of GFP
T NE RT
T NE RT +O HT
n s
SL
SLCHIR
2iL
SLPD
SL2i
B
TNERT
SL
+ OHT
- OHT
SLSU5402
Counts
TDiN
SL
+ Dox
- Dox
SLSU5402
GFP
D
TNERTFgfr1 -/-
Fgfr1 -/-
TNERTFgfr2-/-
Fgfr2 -/-
TNERTFgf4-/-
Fgf4 -/-
TNERTFgfbp1-/-
Fgfbp1 -/-
Randomly integrated
Endogenous Nanog loci
Flag tag
Knockout
Avidin tag
Exon (Coding)
Poly A
Exon (Non-coding)
C
Cell1
Cell2
Cell3
Cell4
Cell5
Cell6
8C
16C
Early blastocyst
Mid blastocyst
Late blastocyst
100
0
E
+ OHT
- OHT
-ve C
TNERTFgfr1-/-
TNERTFgfr2-/-
TNERTFgf4-/-
TNERTFgfbp1-/-
Counts
GFP

**Figure 3**

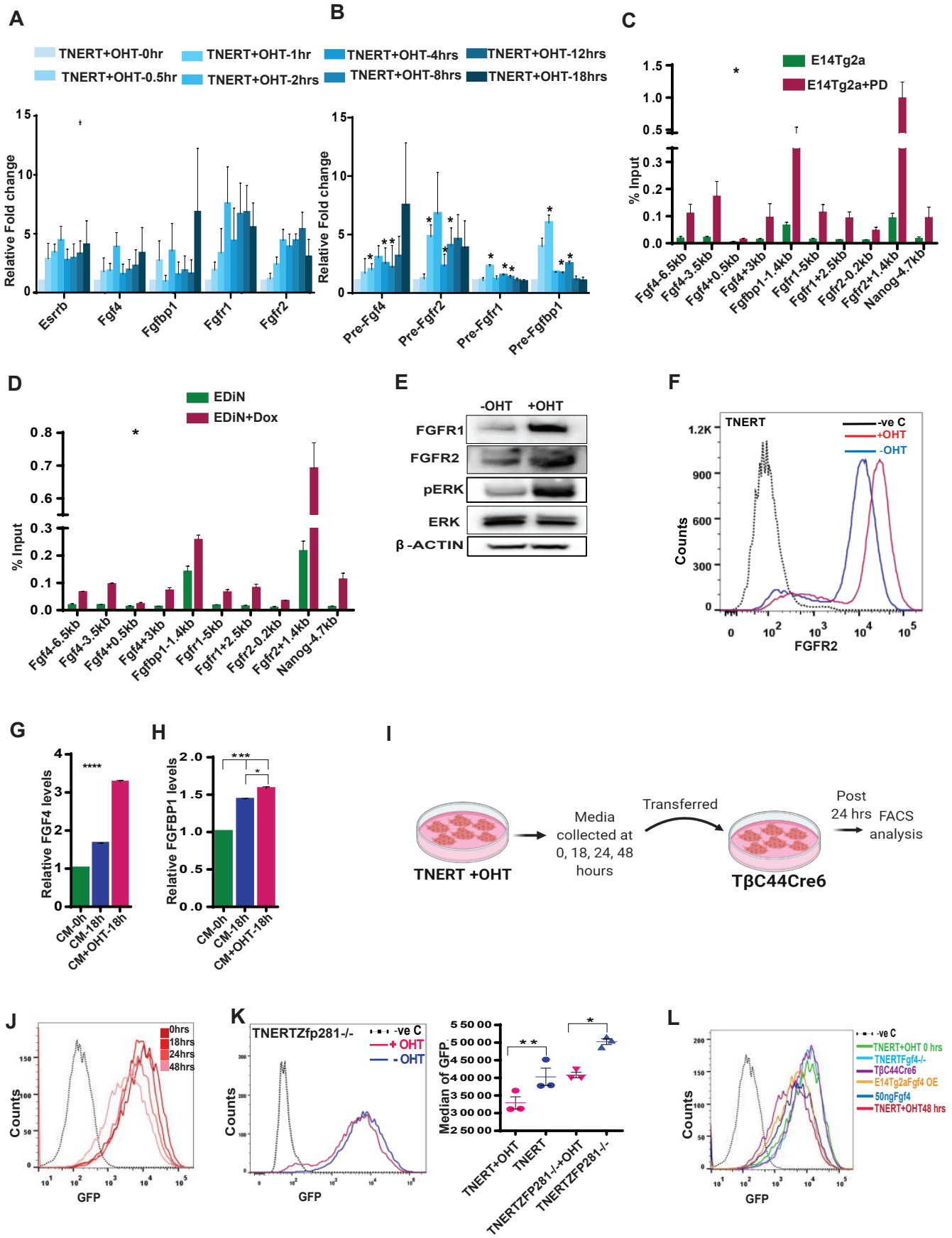
A
TNERT+OHT-0hr
TNERT+OHT-0.5hr
TNERT+OHT-1hr
TNERT+OHT-2hrs
Relative Fold change
Esrrb
Fgf4
Fgfbp1
Fgfr1
Fgfr2
B
TNERT+OHT-4hrs
TNERT+OHT-8hrs
TNERT+OHT-12hrs
TNERT+OHT-18hrs
Relative Fold change
Pre-Fgf4
Pre-Fgfr2
Pre-Fgfr1
Pre-Fgfbp1
C
E14Tg2a
E14Tg2a+PD
% Input
Fgf4-6.5kb
Fgf4-3.5kb
Fgf4+0.5kb
Fgf4+3kb
Fgfbp1-1.4kb
Fgfr1-5kb
Fgfr1+2.5kb
Fgfr2-0.2kb
Fgfr2+1.4kb
Nanog-4.7kb
D
EDiN
EDiN+Dox
% Input
E
-OHT
+OHT
FGFR1
FGFR2
pERK
ERK
β-ACTIN
F
TNERT
-ve C
+OHT
-OHT
Counts
FGFR2
G
Relative FGF4 levels
CM-0h
CM-18h
CM+OHT-18h
H
Relative FGFBP1 levels
CM-0h
CM-18h
CM+OHT-18h
I
TNERT +OHT
Media collected at 0, 18, 24, 48 hours
Transferred
TβC44Cre6
Post 24 hrs
FACS analysis
J
0hrs
18hrs
24hrs
48hrs
Counts
GFP
K
TNERTZfp281-/-
-ve C
+ OHT
- OHT
Counts
GFP
Median of GFP
TNERT+OHT
TNERT
TNERTZFP281-/-+OHT
TNERTZFP281-/-
L
-ve C
TNERT+OHT 0 hrs
TNERTFgf4-/-
TβC44Cre6
E14Tg2aFgf4 OE
50ngFgf4
TNERT+OHT48 hrs
Counts
GFP

## Figure 4

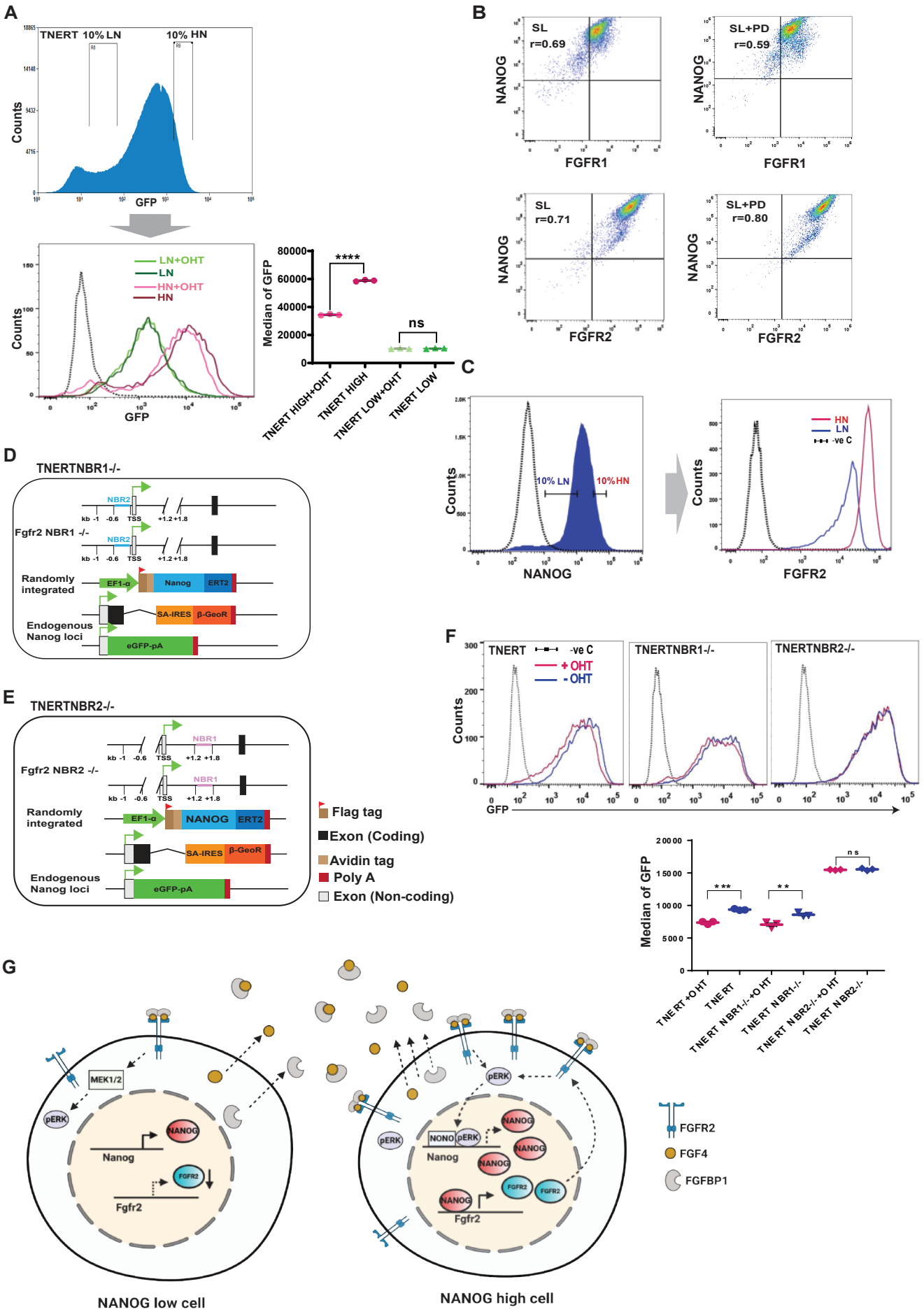
A
TNERT 10% LN
10% HN
Counts
GFP
LN+OHT
LN
HN+OHT
HN
Median of GFP
****
ns
TNERT HIGH+OHT
TNERT HIGH
TNERT LOW+OHT
TNERT LOW
B
SL
r=0.69
SL+PD
r=0.59
SL
r=0.71
SL+PD
r=0.80
NANOG
FGFR1
FGFR2
C
10% LN
10%HN
HN
LN
-ve C
D
TNERTNBR1-/-
Fgfr2 NBR1 -/-
NBR2
kb -1 -0.6 TSS +1.2 +1.8
Randomly integrated
EF1-α
Nanog
ERT2
Endogenous Nanog loci
SA-IRES
β-GeoR
eGFP-pA
E
TNERTNBR2-/-
Fgfr2 NBR2 -/-
NBR1
NANOG
Flag tag
Exon (Coding)
Avidin tag
Poly A
Exon (Non-coding)
F
TNERT
TNERTNBR1-/-
TNERTNBR2-/-
+ OHT
- OHT
Median of GFP
***
**
n s
TNERT +OHT
TNERT
TNERT NBR1-/- +OHT
TNERT NBR1-/-
TNERT NBR2-/- +OHT
TNERT NBR2-/-
G
MEK1/2
pERK
NANOG
Nanog
FGFR2
Fgfr2
NONO
FGF4
FGFBP1
NANOG low cell
NANOG high cell

## Figure 5

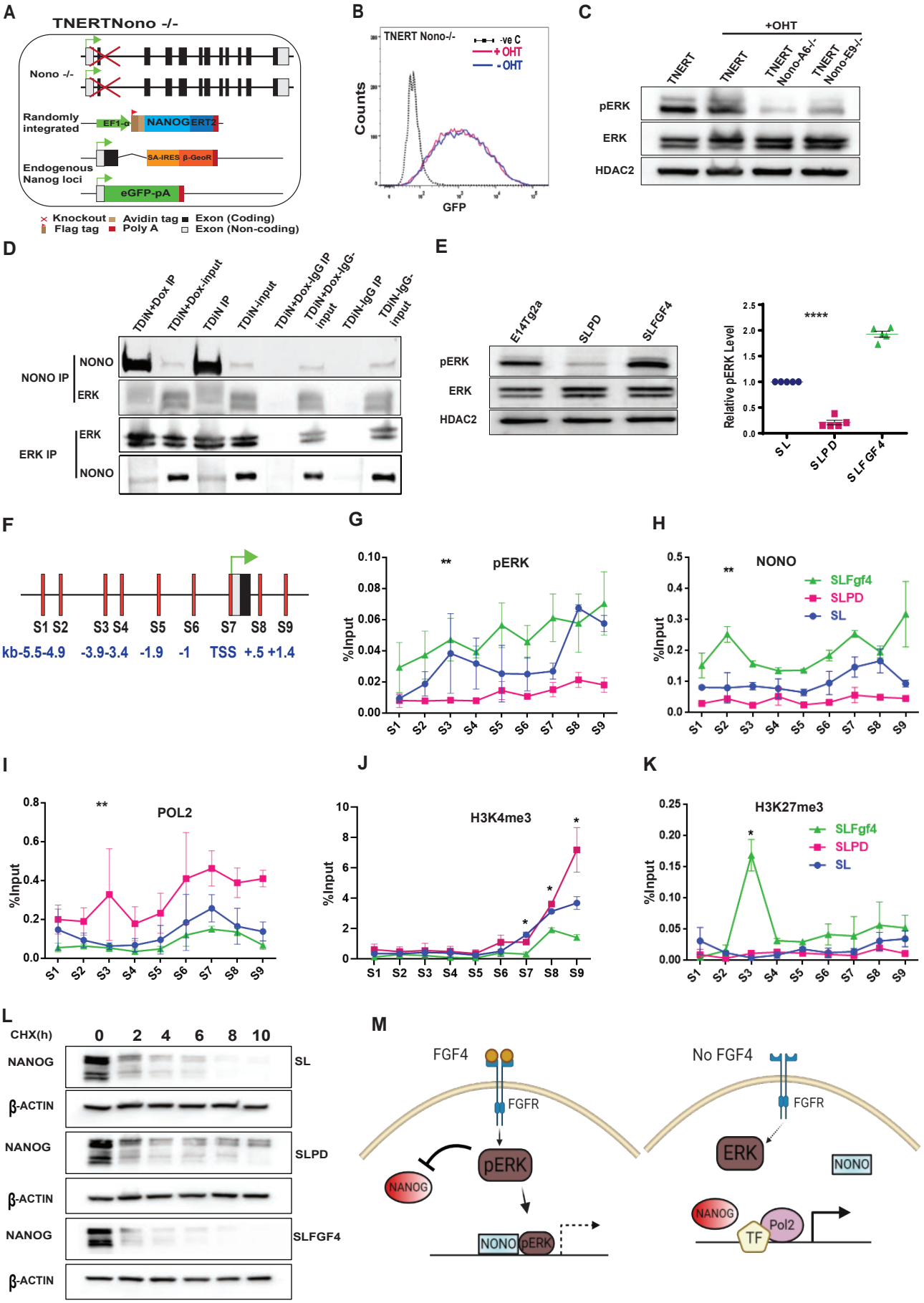
A
TNERTNono -/-
Nono -/-
Randomly integrated
EF1-α
NANOG
ERT2
Endogenous Nanog loci
SA-IRES
β-GeoR
eGFP-pA
Knockout
Avidin tag
Exon (Coding)
Flag tag
Poly A
Exon (Non-coding)
B
TNERT Nono-/-
-ve C
+ OHT
- OHT
Counts
GFP
C
+OHT
TNERT
TNERT
TNERT Nono-A6-/-
TNERT Nono-E9-/-
pERK
ERK
HDAC2
D
TDiN+Dox IP
TDiN+Dox-input
TDiN IP
TDiN-input
TDiN+Dox-IgG IP
TDiN+Dox-IgG-input
TDiN-IgG IP
TDiN-IgG-input
NONO IP
NONO
ERK
ERK IP
ERK
NONO
E
E14Tg2a
SLPD
SLFGF4
pERK
ERK
HDAC2
Relative pERK Level
****
SL
SLPD
SLFGF4
F
S1 S2 S3 S4 S5 S6 S7 S8 S9
kb-5.5-4.9 -3.9-3.4 -1.9 -1 TSS +.5 +1.4
G
pERK
%Input
H
NONO
SLFgf4
SLPD
SL
I
POL2
J
H3K4me3
K
H3K27me3
L
CHX(h) 0 2 4 6 8 10
NANOG
β-ACTIN
SL
SLPD
SLFGF4
M
FGF4
FGFR
pERK
NANOG
NONO
pERK
No FGF4
FGFR
ERK
NONO
NANOG
TF
Pol2

**Figure 6**

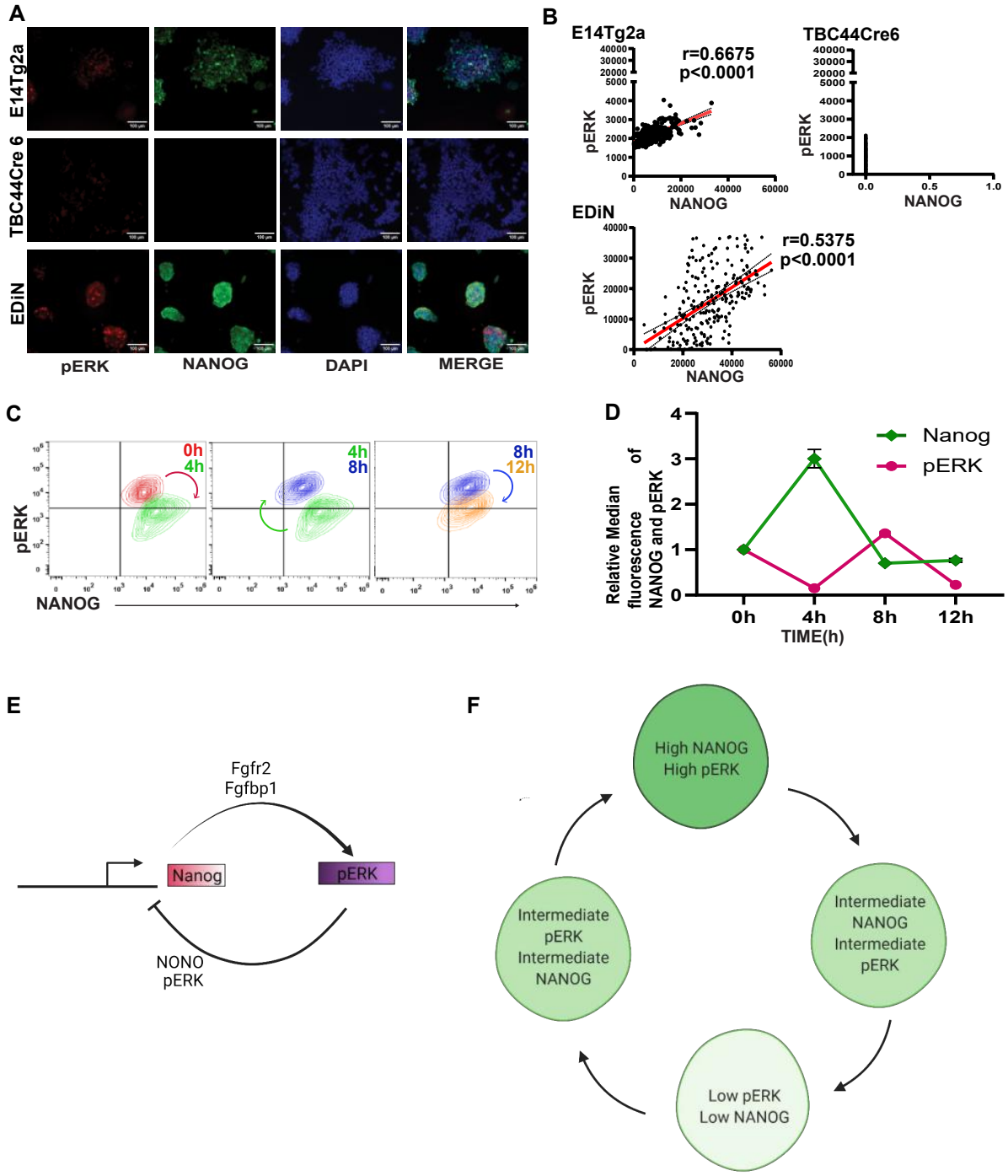
A
E14Tg2a
TBC44Cre 6
EDiN
pERK
NANOG
DAPI
MERGE
B
E14Tg2a
r=0.6675
p<0.0001
pERK
NANOG
TBC44Cre6
pERK
NANOG
EDiN
r=0.5375
p<0.0001
pERK
NANOG
C
0h
4h
4h
8h
8h
12h
pERK
NANOG
D
Nanog
pERK
Relative Median of fluorescence NANOG and pERK
0h
4h
8h
12h
TIME(h)
E
Fgfr2
Fgfbp1
Nanog
pERK
NONO
pERK
F
High NANOG
High pERK
Intermediate
NANOG
Intermediate
pERK
Low pERK
Low NANOG
Intermediate
pERK
Intermediate
NANOG

**Supplementary Information Text**

**Subhead. Materials**

| REAGENT or RESOURCE | SOURCE | IDENTIFIER |
|---|---|---|
| Antibodies | | |
| Anti-NANOG | Thermo Fisher Scientific | Cat# 14-5761-80, RRID: AB_763613 |
| Anti-NANOG | Cell signaling Technology | Cat# 8822, RRID: AB_11217637 |
| Nanog Polyclonal Antibody | Thermo Fisher Scientific | Cat# PA5-47376, RRID: AB_2607022 |
| Anti-OCT3/4 | Cell signaling Technology | Cat# 83932, RRID: AB_2721046 |
| Anti-OCT3/4 | Thermo Fisher Scientific | Cat# 14-5841-82, RRID: AB_914301 |
| Anti-SOX 2 | Cell signaling Technology | Cat# AMAb91307, RRID: AB_2665892 |
| Anti-FGFR2 | Thermo Fisher Scientific | Cat# PA1-24763, RRID: AB_780623 |
| Anti-FGFR2 | R&D Systems | Cat# MAB6843, RRID: AB_2103395 |
| Anti-FGFR1 | Cell signaling Technology | Cat# 9740, RRID: AB_11178519 |
| FGFBP1 Polyclonal Antibody | Thermo Fisher Scientific | Cat# PA5-77220, RRID: AB_2720947 |
| Anti-FGF4 | Thermo Fisher Scientific | Cat# PA5-20483, RRID: AB_11152903 |
| Anti-ERK | Cell signaling Technology | Cat# 9102, RRID: AB_330744 |
| Anti-P-ERK | Cell signaling Technology | Cat# 4370, RRID: AB_2315112 |
| Anti-P-ERK | Cell signaling Technology | Cat#9101, RRID: AB_331646 |
| Anti-Trimethyl Histone H3(Lys4) (C42D8) | Cell signaling Technology | Cat# 9751, RRID: AB_2616028) |
| Anti-Trimethyl Histone H3(Lys27) | Merck Millipore | Cat# 07-449, RRID: AB_310624 |
| Anti- β-ACTIN | Sigma-Aldrich | Cat# A2228, RRID: AB_476697 |
| Anti-HDAC2 | Thermo Fisher Scientific | Cat# 51-5100; RRID: AB_2533908 |
| Anti-RNA polymerase II Antibody, clone CTD4H8 | Merck Millipore | Cat# 05-623, RRID: AB_309852 |
| Chemicals, Peptides, and Recombinant Proteins | | |
| rhFGF4 | R&D Systems | Cat# 7460-F4-025 |
| rhFGFBP1 | R&D Systems | Cat# 1593-FB-025 |
| Human FGF4 recombinant protein | Thermo Fisher Scientific | Cat# PHG0154 |
| Human BMP4 recombinant protein | Thermo Fisher Scientific | Cat# PHC9534 |
| Human EGF recombinant protein | Thermo Fisher Scientific | Cat# 01-107 |
| Human Insulin recombinant protein | Thermo Fisher Scientific | Cat# RP-10908 |

| | | |
|---|---|---|
| Human bFGF recombinant protein | Thermo Fisher Scientific | Cat# RP-8628 |
| G418 disulfate salt | Sigma-Aldrich | Cat# A1720 |
| Doxycycline Hyclate | Sigma-Aldrich | Cat# D9891 |
| SU5402 | Sigma-Aldrich | Cat# SML0443 |
| PD0325901 | Sigma-Aldrich | Cat# PZ0162 |
| CHIR99021 | Sigma-Aldrich | Cat# SML1046 |
| (Z)-4-Hydroxytamoxifen | Sigma-Aldrich | Cat# H7904 |
| LIF | Made in-house | |
| Heparan sulfate sodium salt | Sigma-Aldrich | Cat# H7640 |
| *o*-Phenylenediamine dihydrochloride | Sigma-Aldrich | Cat# P8287 |
| Deposited Data | | |
| | | |
| Experimental Models: Cell Lines | | |
| E14Tg2a | | Chambers et al., 2007 |
| TNGA | | Chambers et al., 2007 |
| TβC44Cre6 | | Chambers et al., 2007 |
| TNERT | This Study | |
| NiRFP2A | This Study | |
| TDiN | This Study | |
| OGNM | This Study | |
| EDiN | This Study | |
| NisGFPDiN | This Study | |
| NsGiR | This Study | |
| TNERTFgfr2-/- | This Study | |
| TNERTFgfr1-/- | This Study | |
| TNERTFgf4-/- | This Study | |
| TNERTFgfbp1-/- | This Study | |
| TNERTNBR1-/- | This Study | |
| TNERTNBR2-/- | This Study | |
| TNERTNono-/- | This Study | |
| E14Tg2aFgf4-/- | This Study | |
| E14Tg2aFgfr2-/- | This Study | |
| E14Tg2aFgf4OE | This Study | |
| Oligonucleotides | | |
| Oligos used for sgRNA cloning, genotyping, qPCR – RTPCR and ChIP-PCR | Supplemental Table 1 | |
| Recombinant DNA | | |
| pU6-(BbsI)-CBh-Cas9-T2A-mCherry | Addgene 64324 | (Weber et al., 2015) |
| Mouse Oct4-GFP GOF18 transgenic reporter | Addgene 60527 | (Gafni et al., 2013) |
| Nanog iRFP670 Fusion Targeting vector | This Study | |
| Nanog sfGFP Fusion Targeting vector | This Study | |
| Nanog-2A-mCherry | Addgene 59995 | (Faddah et al., 2013) |
| pEF6V5His-Fgf4 | This Study | |
| PEF6NanogERT2 | This Study | |
| PTripZ-FaNanog | This Study | |

| | | |
|---|---|---|
| pU6-iRFP | This Study | |
| pU6-iRFP Sg-Fgf4 | This Study | |
| pU6-iRFP Sg-Fgfr1 | This Study | |
| pU6-iRFP Sg-Fgfr2 | This Study | |
| pU6-iRFP Sg-Fgfbp1 | This Study | |
| pU6-iRFP Sg-Zfp281 | This Study | |
| pU6-iRFP Sg-Nono | This Study | |
| pU6-iRFP Sg-Fgfr2-NBR1 | This Study | |
| pU6-iRFP Sg-Fgfr2-NBR2 | This Study | |
| pU6-iRFP Sg-Nanog-Stop | This Study | |
| pMKiN | This Study | |
| Software and Algorithms | | |
| ImageJ | ImageJ | RRID: SCR_003070 |
| FlowJo | BD Bioscience | RRID: SCR_008520 |
| Integrative genomics viewer | Broad Institute | RRID: SCR_011793 |
| SDS | Applied Biosystems | RRID: SCR_015806 |
| Image Lab | Bio-rad | RRID: SCR_014210 |
| GraphPad Prism | GraphPad | RRID: SCR_002798 |
| Other | | |
| Pierce Protein A/G Magnetic beads | Thermo Fisher Scientific | Cat# 88803 |
| BD LSR Fortessa | BD Bioscience | N/A |
| MoFLo XDP | Beckman Coulter | N/A |
| Gallios Flowcytometer | Beckman Coulter | N/A |
| Chemidoc MP imaging system | Bio-rad | |
| Zeiss Axio Observer | Zeiss | N/A |

**Subhead. Methods**

**Cell Culture:** The cell lines used in this study and their origin is depicted in Fig. S7. All the cells used in this study are derivatives of E14Tg2a ES. The cells were cultured as described earlier (5). 4-Hydroxytamoxifen (4-OHT), Doxycycline, and Cycloheximide were used at a concentration of 1 μg/ml, 1 μg/ml, and 100 μg/ml respectively. The TNERT and its derivative cell lines were treated with 4-OHT for 18 hrs except when indicated. TDiN and EDiN were treated with Doxycycline for 48 hrs unless indicated. CHIR99021 (CHIR, PD0325901 (PD), and SU5402 were used at 3 μM, 1 μM, and 2 μM, respectively, except when indicated. FGF4 and FGFBP1 were used at 50ng/ml concentration. The cells were cultured in Serum+ LIF (SL), SL+ PD (SLPD), SL+CHIR (SLCHIR), SL+SU5402 (SLSU5402), SL + PD +CHIR (SL2i) and N2B27+LIF+PD+CHIR (2iL) for at least 2 passages before treating with either 4-OHT or Doxycycline.

The cells were cultured on cell culture dishes coated with 0.1% gelatin for all experiments. The conditioned media from the cells was collected after the specific treatments or indicated time

points. The conditioned media was passed through a 0.22 μM filter and added to Tβc44Cre6 or TNERT cells. The cells were cultured in the conditioned media for 24 hrs before FACS analysis.

**Generation of Knock-out cell lines using paired CRISPR constructs:** pU6-iRFP (pU6-Cas9-T2A-iRFP-2A-PuroR) construct was engineered by replacing mCherry coding sequence with iRFP670-2A-PuroR cassette in pU6-(BbsI)-CBh-Cas9-T2A-mCherry plasmid (Addgene 64324) by Gibson assembly. For generating knock-out of a gene, two sgRNAs were designed with the expected cutting sites at least 30 bps apart to achieve deletion of at least 30 bps or more. For genotyping of the deletions, a set of genotyping primers was designed outside the deletion region flanking the sgRNA pair. The sgRNAs were designed using the UCSC genome browser and Deskgen or Benchling. The sequences of the sgRNAs and the genotyping primers are detailed in Table S1. All sgRNAs were cloned into pU6-Cas9-T2A-iRFP-2A-PuroR plasmids. To generate a paired sgRNA construct, the U6-SgRNA cassette from one plasmid containing the sgRNA was amplified and Gibson assembled into the XbaI site of the plasmid containing the other sgRNA pair of the pair. Around 1 µg of paired sgRNA CRISPR plasmid was nucleofected in 1 million cells. The transfected cells were sorted by FACS for iRFP expression and cultured to obtain clones. The clones were genotyped by PCR using respective primer sets to identify the heterozygous and homozygous clones. The sequence of the derivation of cell lines is described in Fig. S7.

**Western blot analysis:** The cells were harvested by using RIPA buffer with 25mM Tris HCl (pH 8.0), 150mM NaCl, 1%NP-40, 0.5% Sodium deoxycholate, 0.1% SDS and Complete Protease Inhibitor Cocktail Tablets (Roche). The protein samples were resolved by 4-20% gradient SDS-PAGE and electroblotted on to polyvinylidene difluoride (PVDF) membrane. The blot was blocked with 3% Blotto for an hour and incubated overnight with a primary antibody at 4°C. Blots were washed thrice with TBST and hybridized with secondary antibody and the blots were visualized using enhanced chemiluminescence (ECL)detection kit. Western blot quantifications were performed using Image lab (Bio-rad).

**Chromatin Immunoprecipitation (ChIP):** Cells were fixed by adding 270 µL of 37% formaldehyde into 10 ml of media and incubated for 10 minutes at 37°C to crosslink the chromatin. Cells were washed twice with cold PBS containing protease inhibitors. Cells were scraped and harvested by centrifugation. The cell pellet was dissolved in 200 µL of SDS Lysis Buffer (1% SDS, 10 mM EDTA, and 50 mM Tris, pH 8.0) containing protease inhibitors (per $10^6$ cells) and incubated on ice for 10 min. The 25 cycles of sonication were used to shear DNA between 200 to1000 base pairs. The sample was centrifuged at 13,000 rpm for 10 min (at 4°C). The supernatant was diluted by adding 1800 µl ChIP Dilution Buffer (1.1% Triton X- 100, 1.2 mM EDTA, 16.7 mM Tris-HCl, pH 8.0, 167 mM NaCl with protease inhibitors). The 1% input was aliquoted from the supernatant. To reduce nonspecific background, diluted cell supernatant was preabsorbed for one hour at 4°C with protein

A/G magnetic beads (Invitrogen). The supernatant fraction was incubated overnight at 4°C with an appropriate antibody and protein A/G magnetic beads were blocked with 4% BSA, 2µg salmon sperm DNA. The next day, pre-blocked beads were mixed with the sample and incubated for 1 hour to capture the antibodies. The supernatant was discarded and washed in the given order with 1 mL of each of the buffers - Low Salt Wash Buffer (0.1% SDS, 1% Triton X-100, 2 mM EDTA, 20 mM Tris-HCl, pH 8.0, 150 mM NaCl), High Salt Wash Buffer (0.1% SDS, 1% Triton X-100, 2 mM EDTA, 20 mM Tris-HCl, pH 8.0, 500 mM NaCl), LiCl Wash Buffer (0.25 M LiCl, 1% IGEPAL-CA630, 1% deoxycholic acid, 1 mM EDTA, 10 mM Tris, pH 8.0.), and TE buffer. DNA was eluted with elution buffer (1%SDS, 0.1M NaHCO3). The sample input and the ChIP chromatin were reverse crosslinked with 20 µL of 5 M NaCl by heating at 65°C for 4 hours. Followed by one hour at 45°C with 10 µL of 0.5 M EDTA, 20 µL 1 M Tris- HCl, pH 6.5, and 2 µL of 10 mg/mL Proteinase K. Finally, DNA was eluted in 50 µL water using a minEleute PCR purification kit. Then 1µL of sample and input was used for qPCR analysis. The primers used for qPCR analysis were listed in Table S1.

**Co-Immunoprecipitation in ES cells:** 10-12 million ES cells were harvested by trypsinization, washed twice with cold PBS, and resuspended in 800 µl of CoIP Lysis Buffer (50 mM Tris-HCl, pH 67.5; 350 mM NaCl, 0.7% NP40, EDTA 0.1mM, 20% (v/v) glycerol, and protease inhibitor cocktail). The cell lysate was mixed with protein A/G magnetic beads for 1 hour at 4ºC for pre-clearing the background. Then 5% input was aliquoted and the remaining supernatant was incubated overnight with appropriate primary antibody. The protein A/G magnetic beads were blocked overnight at 4ºC with 200 µl of CoIP Lysis buffer containing 4% BSA. The next day, the beads were transferred to the primary antibody incubated tubes and incubated for one hour at 4ºC. The bead was washed three times with ice-cold TBS150 (50mM Tris, 150mM NaCl) and the protein was eluted with 2X sample buffer (125 mM Tris-HCl, pH 6.8**,** 4% SDS**,** 20% (v/v) glycerol, 0.004% bromophenol blue), by boiling for 5 min. The western was done for sample and input and the interaction was analyzed.

**Immunocytochemistry:** The cells were cultured in 24 well dishes and fixed in 3.7% formaldehyde diluted in PBS for 15 mins at RT. After 3 washes with PBS, the cells were permeabilized and blocked with PBS containing 0.5% BSA and 0.3% Triton-X100 for 1 hour at room temperature. The cells were hybridized with primary antibody (1:100 dilution) in PBS containing 0.5% BSA at 4ºC overnight in a humidified chamber. The cells were washed three times with PBS and hybridized to appropriate secondary antibody at 1:1000 dilution room temperature for 1hour. The nuclei were stained with DAPI in 1X PBS for 20 min at room temperature. The cells were washed thrice with PBS. The cells were layered with 100 µl of the mixture of PBS and Glycerol (1:1) and the images were acquired on the ZEISS Axio observer microscope and analyzed using ImageJ software.

**ELISA Assay:** The condition media from the cell lines was collected at the respective time points. 100 µl of the media was coated per well of 96 wells of ELISA plate by incubating overnight at 4$^{o}$C. The wells were washed thrice with PBS containing 0.05% Tween-20 and blocked with PBS containing 2% BSA for one hour at room temperature. The wells were washed once with PBS and incubated with the appropriate primary antibody (1:100) for one hour. Washed thrice with PBST, an appropriate HRP-labeled secondary antibody was hybridized for one hour at room temperature. The wells were washed thrice with PBST and incubated in substrate solution OPD (o-phenylenediamine dihydrochloride) 3mg/ml with 6 µl/ml $H_2O_2$) for 30 min in dark. The reaction was stopped by using 2N $H_2SO_4$. The absorbance was measured at 492 nm in Power wave XS2 (Bio Tek instruments).

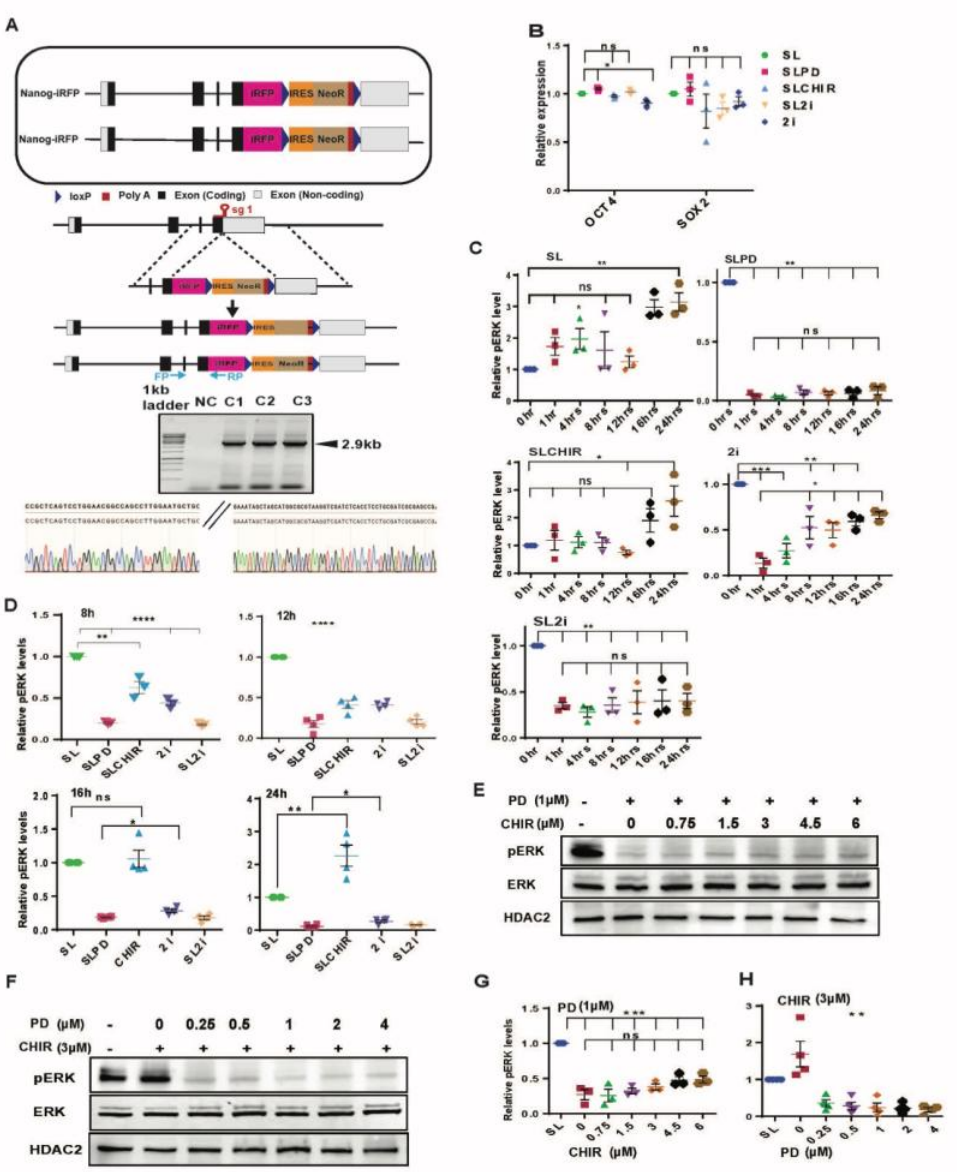


**Fig. S1. Residual MEK1/2 activity in the ground state prevents complete derepression of *Nanog*.** (A) (top) Schematic depiction of NiRFP2A with both alleles of *Nanog* fused to iRFP coding sequences in frame with last coding sequence. (Middle) CRISPR mediated knock-in strategy of the iRFP-loxP-IRES-NeoR-loxP cassette into *Nanog* locus. The sgRNA includes the stop codon of the *Nanog* gene. The location of the genotyping primers (FP/RP) for the knock-in is marked by the arrows. (Bottom) Genotyping of the NiRFP2A clones, a 2.9 kb band is amplified only in the knock-in clones as one of the primers is complementary to a sequence outside the left homology arm and the other primer is complementary to the iRFP sequence. (B) Relative quantification of OCT4 and SOX2. The expression is normalized relative to HDAC2 levels and expression levels of OCT4 and SOX2 in SL (n>=3). (C, D) Relative pERK expression levels in indicated time points and treatments (n=3). (E) Western blot of pERK and ERK in 1 $\mu$M PD and increasing concentrations of CHIR in SL media. (F) Western blot of pERK and ERK in 3 $\mu$M CHIR and increasing concentrations of PD in SL media. (G, H) Relative pERK expression levels in indicated concentrations of CHIR and PD respectively (n>=3). All error bars in the figure represent s.e.m..

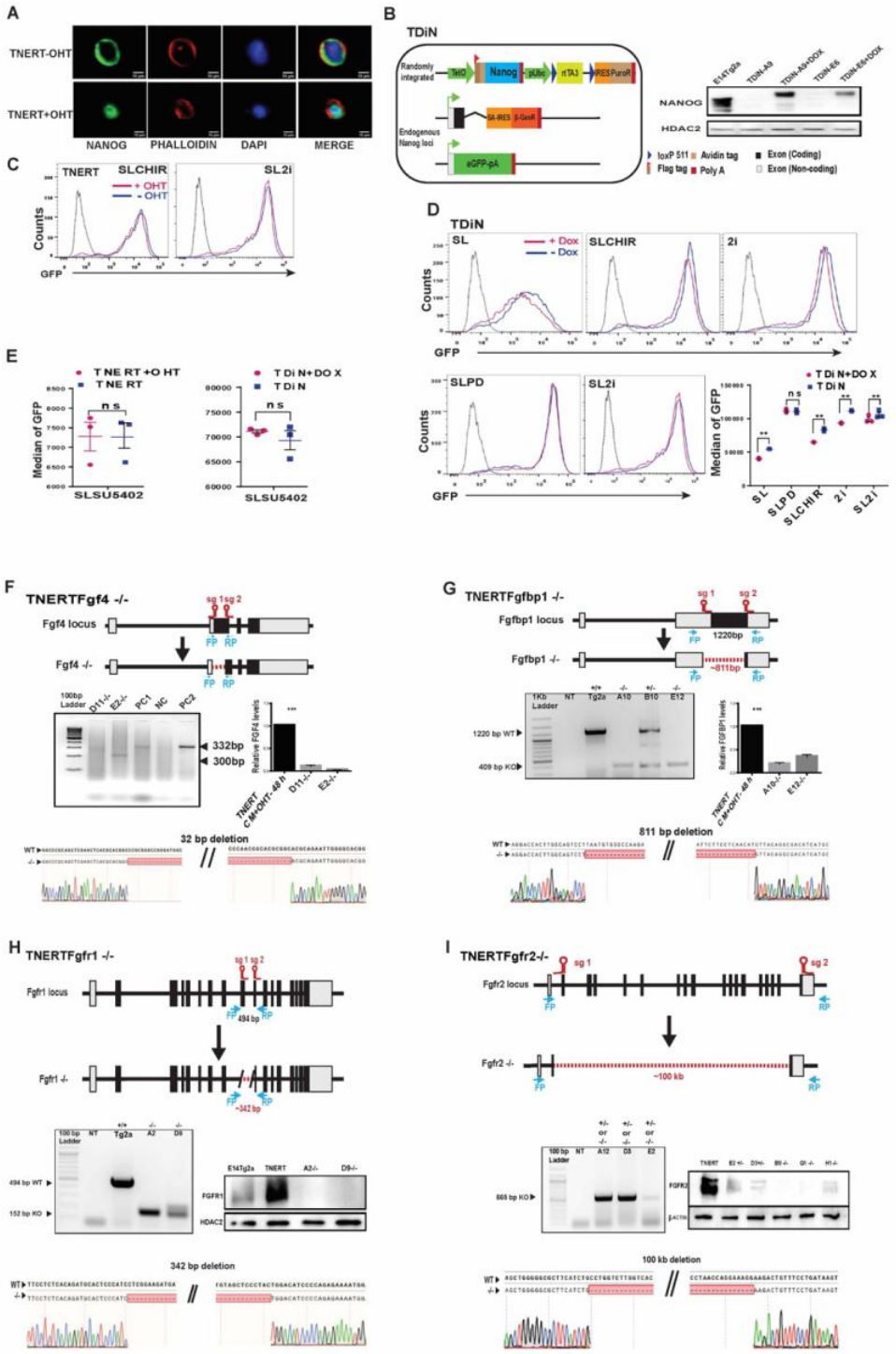


**Fig. S2. FGF autocrine signaling pathway components are essential for *Nanog* autoregulation.** (A) Immunofluorescence of NANOG in TNERT cells after 30 mins treatment with or no OHT. Scale bars represent 10μM. (B) (left) Schematic of Doxycycline inducible TDiN cell line, generated by the introduction of a Tetracycline inducible Flag-Avi-NANOG (FaNANOG) transgene in Tβc44Cre6 cell line. (Right) Western blot of FaNANOG in TDiN cells after 48 hrs treatment with or no Doxycycline. (C) FACS profiles of TNERT treatment with or no OHT in SLCHIR and SL2i. D) FACS profiles of TDiN cell line in SL, SLCHIR, 2i, SL2i, and SLPD, (bottom right) *Nanog*:GFP

population median of TDiN in indicated treatments (n=3). (E) *Nanog*:GFP population median of TNERT, NsGFPDiN, and TDiN treated with SU5402, with OHT/Doxycycline or no OHT/Doxycycline. (F) (top) CRISPR-based knock-out strategy using paired sgRNA to knock-out *Fgf4* in TNERT. The sgRNAs are positioned at the beginning and the near end of exon II. The deletion results in the loss of the start codon and a part of the coding region in exon II. The dotted line represents the deleted region of the gene. FP and RP represent the relative positions of the genotyping primers. (Middle left) genotyping PCR of TNERTFgf4-/- clones. The WT allele gives an amplicon of 332 bp and the knock-out allele a smaller amplicon by 32 bps or more. (Middle right) The relative abundance of FGF4 in media of TNERT and TNERTFgf4-/- clones 48 hrs after OHT treatment. (Bottom) Chromatogram of the TNERTFgf4-/- clones showing the sequences at the junction of the deletion. (G) (top) Schematic of the gene structure of *Fgfbp1* and the relative positions of the two sgRNAs used for paired sgRNA knock-out strategy. One sgRNA is complimentary to 5'UTR and the other to the 3' end of the coding region of the only exon. (Middle left) Genotyping PCR showing a WT amplicon of 1220 bps and an amplicon around 400 bps in case of deletion. (Middle right) The relative abundance of FGFBP1 in media of TNERT and TNERTFgfbp1-/- clones 48 hrs after OHT treatment. (Bottom) Chromatogram of the TNERTFgfbp1-/- clone showing the sequences at the junction of the deletion. (H) Strategy for knock-out of *Fgfr1* in TNERT cells. The schematic depicts the gene structure of *Fgfr1* with the relative positions of the two sgRNAs. One sgRNA targets the 3'end of Intron 8 and the other exon10. (Middle left) Genotyping PCR shows a WT allele amplicon at 494 bp and a knock-out allele with smaller amplicons around 150 bp. (Middle right) Western blot analysis of FGFR1 in TNERT and TNERTFgfr1-/- clones. (Bottom) chromatogram showing the sequence of the deleted region. (I) A paired sgRNA strategy to knock-out *Fgfr2* in TNERT. (Top) The schematic represents the *Fgfr2* gene structure, with relative positions of the sgRNAs. One sgRNA target exon2 and the other sgRNA targets the coding region of the last exon approximately 100 kb apart. The dotted line represents the region of deletion in the *Fgfr2* gene. (Middle left) PCR genotyping shows a 665 bp amplicon when at least one allele of *Fgfr2* is deleted. This genotyping strategy cannot distinguish between +/- and -/- genotypes. (Middle right) Western blot analysis of FGFR2 protein in the *Fgfr2* targeted clones distinguishing the +/- and -/- clones. (Bottom) chromatogram represents the sequence of the genotyping amplicon indicating the exact sites of deletion. All error bars in the figure represent s.e.m.

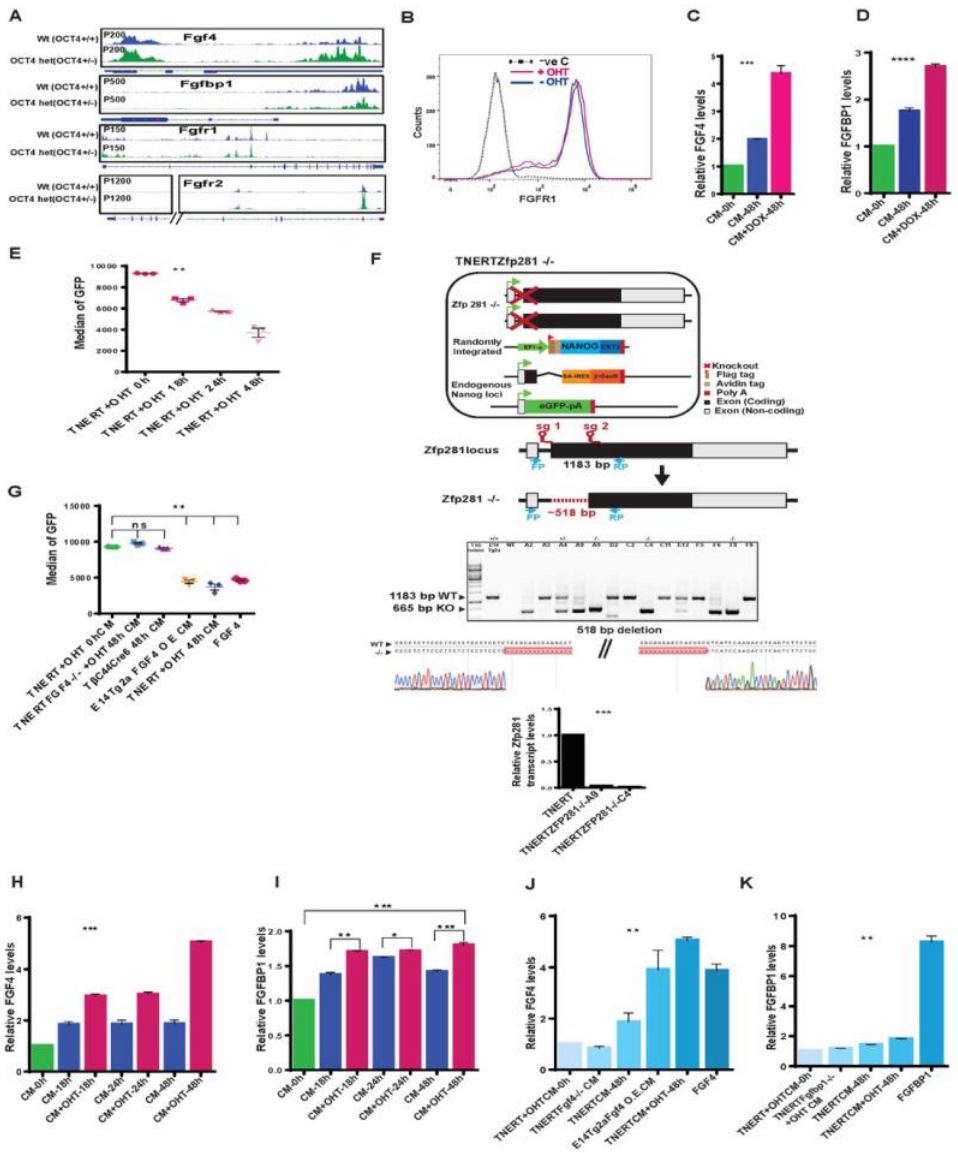


**Fig. S3. *Nanog* enhances expression of FGF autocrine signaling pathway components.** (A) Browser tracks of NANOG enrichment in Fragment Per Kilobase of transcripts per Million (FPKM) in Oct4+/+ cells (normal NANOG levels) and Oct4+/- cells (higher NANOG levels) (Karwacki-Neisius et al., 2013) at *Fgf4, Fgfbp1, Fgfr1,* and *Fgfr2* loci. (B) Histogram of FGFR1 expression on the cell surface analyzed by immunostaining and FACS of fixed but unpermeabilized TNERT cells treated with (red) or no OHT (blue). (C, D) ELISA-based relative quantification of FGF4 and FGFBP1in media from EDiN cells cultured with or no Doxycycline (n=3). EDiN cell was generated by introducing a Doxycycline inducible Flag-Avi-NANOG transgene in E14Tg2a cells. (E) *Nanog*:GFP population median of Tβc44Cre6 treated with OHT induced conditioned media collected after different time points (n=3). (F) (top) Schematic of TNERTZfp281-/- cells, (upper-middle) CRISPR based paired guide knock-out strategy indicating the relative position of the sgRNAs, FP and RP indicate the genotyping primers. (Lower middle) Genotyping PCR indicating +/- and -/- clones. (Bottom) The sequencing chromatogram of the deleted region confirms the exact site of deletion, followed by RT-qPCR analysis of the *Zfp281* transcripts. (G) *Nanog*:GFP population median of Tβc44Cre6 treated with conditioned media from TNERT+OHT 0 hrs, TNERTFGF4-/- +OHT 48 hrs, Tβc44Cre6 48 hrs, E14Tg2a-FGF4-OE (overexpression) 48 hrs, TNERT+OHT 48 hrs and 50ng/ml FGF4 (n=3). (H, I) ELISA-based relative quantities of FGF4 and FGFBP1 in media

from TNERT after 18, 24, and 48 hrs of OHT treatment (n=3). (J) ELISA-based relative quantities of FGF4 in conditioned media from cell lines -TNERT+ OHT 0 hrs, TNERTFGF4-/- + OHT 48 hrs, E14Tg2a-FGF4-OE 48 hrs (overexpression), TNERT-/+OHT 48 hrs, and 50ng/ml FGF4 (n=3). (K) ELISA-based relative quantities of FGFBP1 in conditioned media from various cell lines - TNERT+ OHT 0 hrs, TNERT-Fgfbp1-/- 48 hrs +OHT, TNERT 48 hrs -/+ OHT, and 50 ng/ml FGBP1 (n=3). All error bars in the figure represent s.e.m.

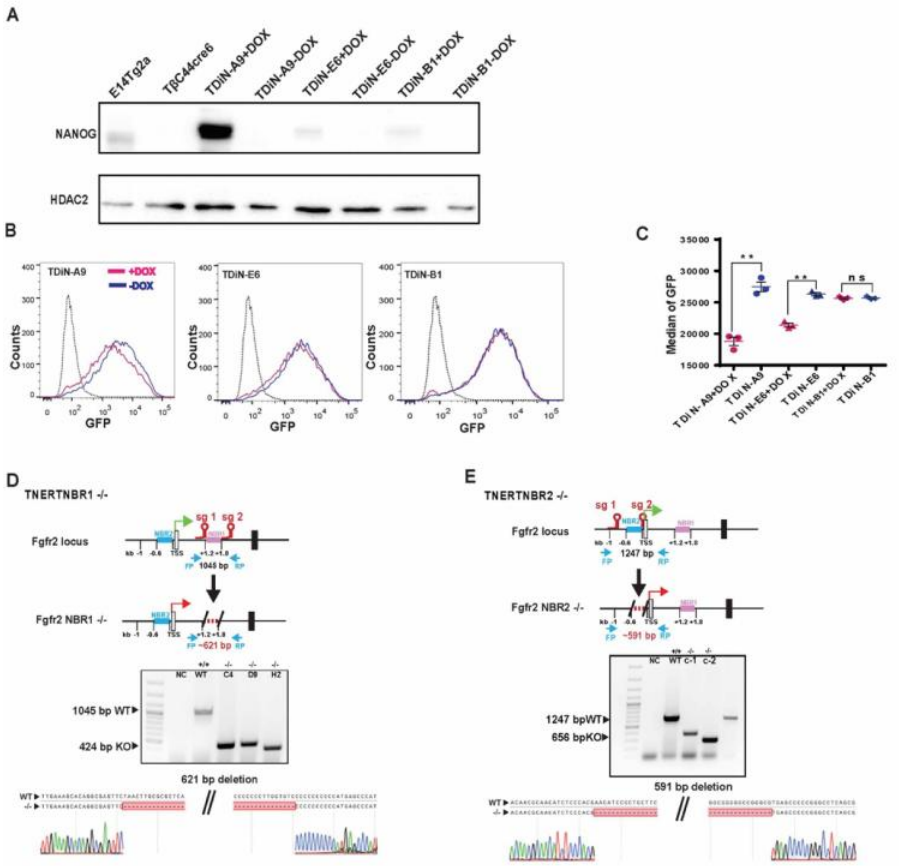


**Fig. S4. NANOG induced FGFR2 triggers autoregulation predominately in the ES cell population with higher *Nanog* expression.** (A) Western blot analysis of Flag-Avi-NANOG in different clones of TDiN treated with or no Doxycycline showing different levels of NANOG expression relative to E14Tg2a. The clones show different levels of expression Flag- Avi-NANOG upon Doxycycline treatment. (B) FACS profiles of *Nanog*:GFP in TDiN clones treated with or no Doxycycline. (C) *Nanog*:GFP population median of TDiN clones (n=3). (D) (top) Schematic of strategy for deletion of NANOG Binding Region 1 (NBR1) in TNERT indicating the position of the NBR1 and the relative position of the sgRNA pair. The sgRNAs are complementary to sequences around 1.2 kb and 1.8 kb downstream of TSS. FP and RP indicate the relative position of the primers for genotyping. (middle) Genotyping of TNERT NBR1 knock-out clones. The WT shows an amplicon of 1045 bp, upon deletion around 600 bp sequence comprising multiple NANOG binding sites is deleted. (bottom) Sequence and chromatogram of the genotype PCR amplicon indicating the exact sequence of the junction of deletion in TNERTNBR1-/- clone. (E) Schematic of strategy for deletion of NANOG Binding Region 2 (NBR2) in TNERT indicating the position of NBR2 and relative position of the sgRNA pair. The sgRNAs are complementary to sequences around TSS and 0.6 kb upstream of TSS of *Fgfr2*. (middle) Genotyping of the TNERTNBR2 knock-out clones. The WT shows an amplicon of 1247 bp. The knock-out would lead to deletion of around 690 bps and a smaller amplicon of around 650 bps. (bottom) Sequence and chromatogram of the PCR amplicon from TNERT knock-out clones showing the exact site of deletion in TNERT NBR2-/- clone. All error bars in the figure represent s.e.m.

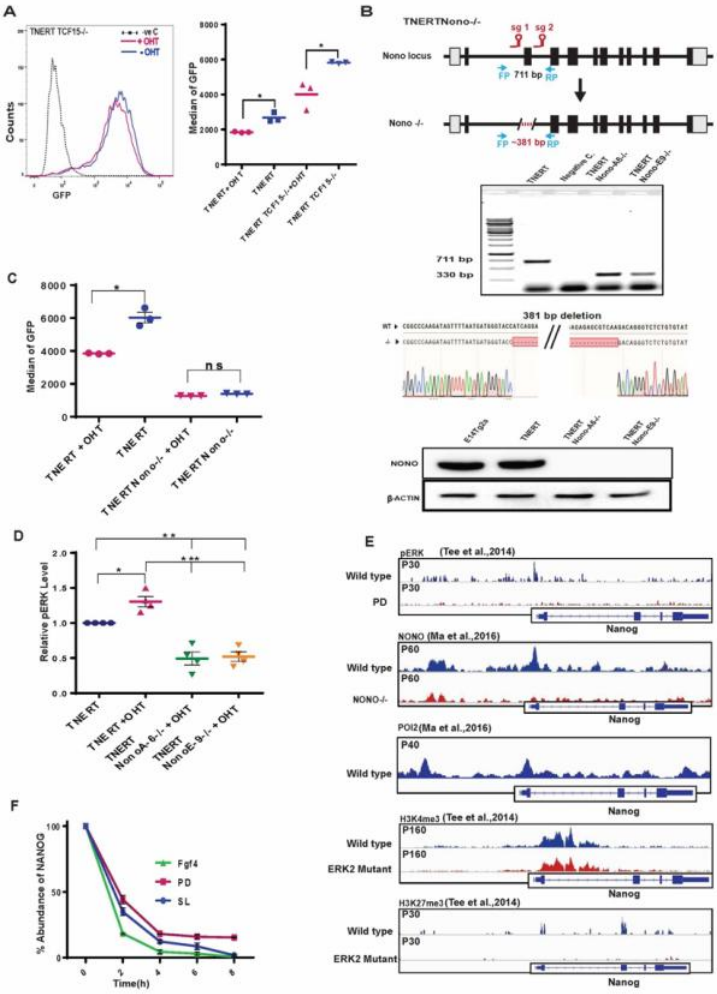


**Fig. S5. ERK interacts and recruits NONO to repress Nanog transcription.** (A) (Left) FACS profile of TNERTTcf15-/- treated with or no OHT (n=3). (Right) *Nanog*:GFP population median of TNERT and TNERTTcf15-/--/- treated with or no OHT (n=3). (B) A CRISPR-based knock-out strategy using paired sgRNA, to knock-out of *Nono* in TNERT cells. (Top) The schematic represents the mouse *Nono* gene structure with relative positions of the two sgRNAs flanking the second coding exon of *Nono*. FP and RP indicate the relative position of genotyping primers. The dotted line indicates the region of deletion in the *Nono* gene. (Middle) Genotyping PCR of the *Nono*-/- deletion in TNERT. The WT allele gave an amplicon of 711 bp and the deleted allele shows a smaller amplicon of 330 bp; followed by sequence and chromatogram indicating the deletion site (bottom) Western blot analysis of NONO protein in TNERT and TNERTNono-/- clones. ( C ) *Nanog*:GFP population median of TNERT and TNERTNono-/- treated with or no OHT (n=3). (D) The relative abundance of pERK in TNERT treated with or no OHT and TNERTNono-/- with OHT (n=4). (E) Browser tracks of pERK, NONO, POL2, H3K4me3, H3K27me3 enrichment in Fragment Per Kilobase of transcripts per Million (FPKM) on *Nanog* gene (Ma et al., 2016; Tee et al., 2014). (F) The relative abundance of NANOG after 0, 2, 4, 6, and 8 hrs of Cycloheximide (CHX) chase cultured in SL, PD, and FGF4 (n=3). All error bars in the figure represent s.e.m.

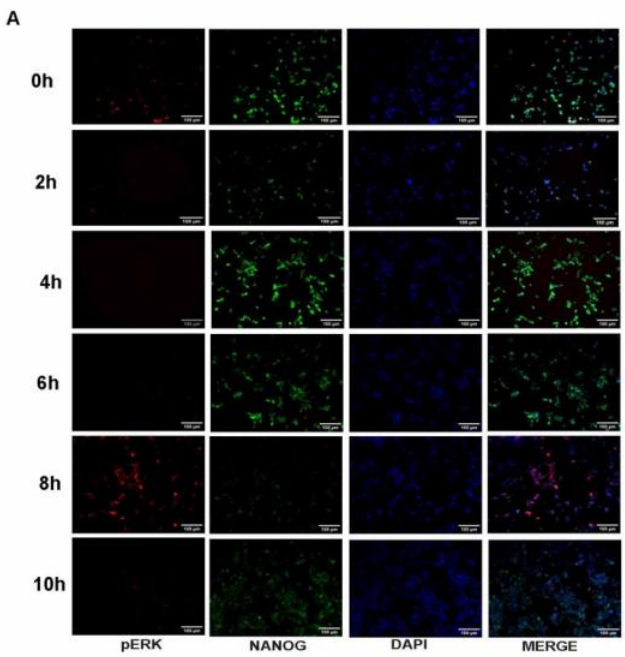


**Fig. S6. NANOG regulates ERK signaling dynamics and heterogeneity.** (A) Immunocytochemistry at different time intervals of culture of NiRFP2A ESCs after sorting of 10% of *Nanog*-high cells. pERK (red), NANOG (green) and nuclear stain (blue). pERK and NANOG were detected in 10% *Nanog*-high cells immediately after sorting. Some of the cells expressed both pERK and NANOG. pERK decreased drastically within 2 hrs of culture. pERK1//2 was lowest at 4 hrs with concomitant high expression of NANOG. pERK expression was increased by 8 hrs coinciding with decreased NANOG. The pERK expression decreased by 10 hrs with increase in NANOG.

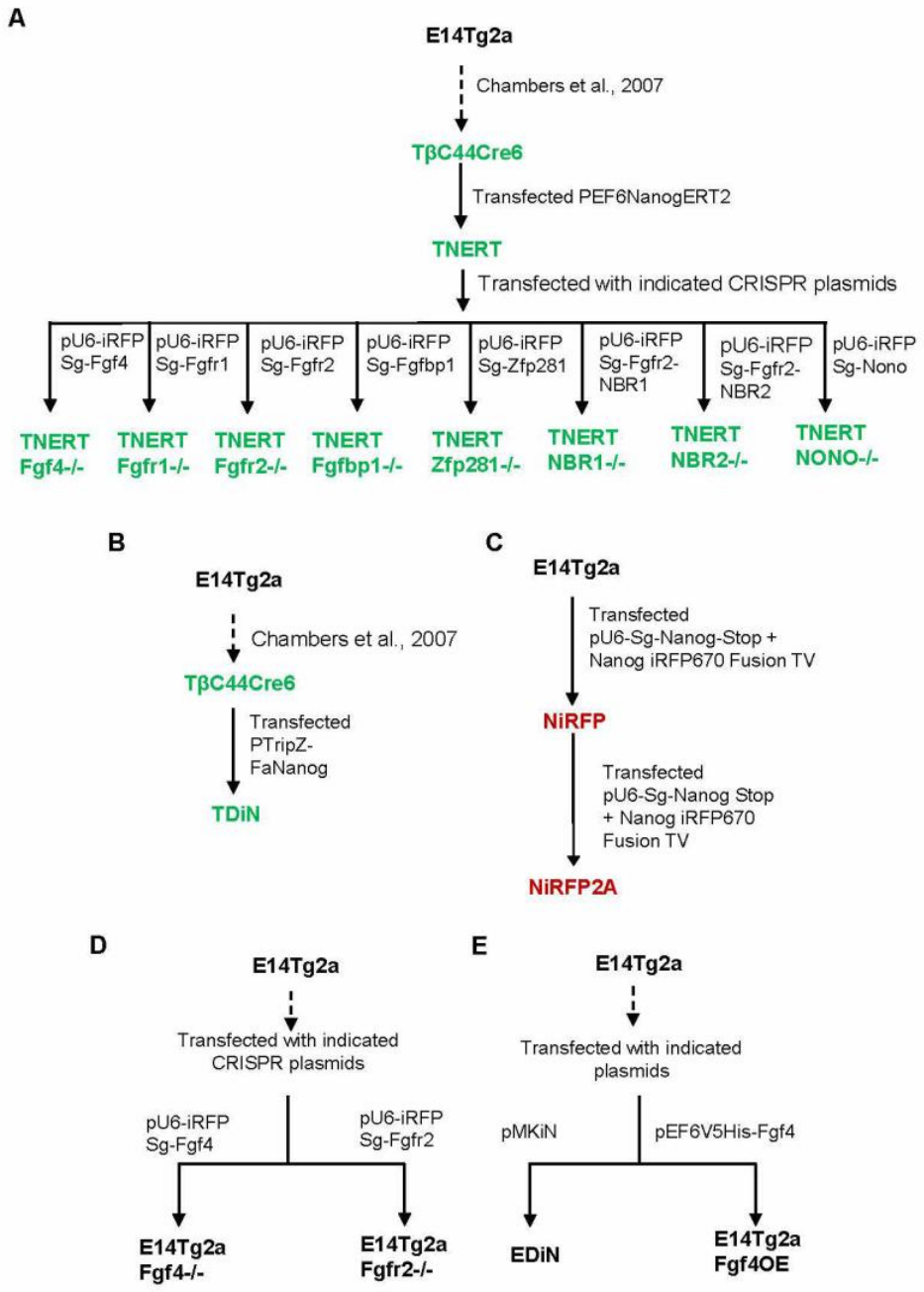


**Fig. S7: A pedigree chart of cell lines used in this study.** (A) Flow chart illustrating the lineage and process of generation of TNERT and generation of knock out cells lines in TNERT background. (B) A flow chart describing derivation of TDiN. (C) A flow chart depicting derivation of NiRFP2A from E14Tg2a. (D) A flow chart depicting derivation of *Fgf4*-/- and *Fgfr2*-/- ES cell lines from E14Tg2a. (E) A flowchart depicting derivation of EDiN and *Fgf4*OE (over expression) ES cell lines from E14Tg2a.

**Table S1**. **Oligonucleotide sequences used in this study**.

| Name of the Oligo | Sequence |
|---|---|
| **Oligos for paired sgRNA Knock-out** | |
| Fgf4 sgRNA1 | CACCGCCGTGCGTGAGTTCGAGCTG |
| | AAACCAGCTCGAACTCACGCACGGG |
| Fgf4 sgRNA2 | CACCGCGAAACGCGGGCCGACCAC |
| | AAACGTGGTCGGCCCGCGTTTCGC |
| Fgfr1 sgRNA1 | CACCGCGTCATCATCTTCCGAGGAT |
| | AAACATCCTCGGAAGATGATGACGC |
| Fgfr1 sgRNA2 | CACCGTTCTCTGGGGATGTCCAGTA |
| | AAACTACTGGACATCCCCAGAGAAC |
| Fgfr2 sgRNA1 | CACCGCTGGGGGCGCTTCATCTGCC |
| | AAACGGCAGATGAAGCGCCCCCAGG |
| Fgfr2 sgRNA2 | CACCGCTCAGTGTAAGTAGGTTCC |
| | AAACGGAACCTACTTACACTGAGC |
| Fgfbp1 sgRNA1 | CACCGCACAGTCTTGGCCCACATTA |
| | AAACTAATGTGGGCCAAGACTGTGC |
| Fgfbp1 sgRNA2 | CACCGATGTCGCCTGTAACATGTTG |
| | AAACCAACATGTTACAGGCGACATC |
| Fgfr2 NBR1 sgRNA1 | CACCGTCGGAGCAGCTAGGCGAACT |
| | AAACAGTTCGCCTAGCTGCTCCGAC |
| Fgfr2 NBR1 sgRNA2 | CACCGTTGTGTTTAGGGCCCCCCCT |
| | AAACAGGGGGGGCCCTAAACACAAC |
| Fgfr2 NBR2 sgRNA1 | CACCGTGGAAGCAGCGGATGTTCGT |
| | AAACACGAACATCCGCTGCTTCCAC |
| Fgfr2 NBR2 sgRNA2 | CACCGACCGGAGCTGCTCTCGGATC |
| | AAACGATCCGAGAGCAGCTCCGGTC |
| Nanog -stop codon sgRNA | CACCGTATGAGACTTACGCAACATC |
| | AAACGATGTTGCGTAAGTCTCATAG |
| Zfp281 sgRNA1 | CACCGAGGCCTGGCTGCGGAGAGG |
| | AAACCCTCTCCGCAGCCAGGCCTC |
| Zfp281 sgRNA1 | CACCGCGGGGTATGAAAATCGGCAG |
| | AAACCTGCCGATTTTCATACCCCGG |
| Nono sgRNA1 | CACCGTTTTAATGATGGGTACCATC |
| | AAACGATGGTACCCATCATTAAAAC |
| Nono sgRNA1 | CACCGTTCCGAGAGAGCGTCAAGAC |
| | AAACGTCTTGACGCTCTCTCGGAAC |
| **Genotyping primers** | |
| Fgf4 knock-out | CGCAGCACTCACCGAACTCA |
| | TGCCCACGTTGCAGTAGAGC |
| Fgfr1 knock-out | GTCTAGACAGGGCGAATGCTGTTT |
| | ACTTGAACTTCACCGTCTTGGCAG |
| Fgfr2 knock-out | TCTGGGTTTAAGCAAGTTGGCACT |
| | CAGCATACATGGTGGGTCAGAGAG |
| Fgfbp1 knock-out | GAAAGTGAGAAGCTGAGTGAATGG |
| | TATATGCACCTAGGTTTGTGGTCC |
| Fgfr2 NBR1 knock-out | GAAGAAACTGCTGGAGTGTGGTCA |
| | AGGGTAGTTCCAGGATACCTCAGC |
| Fgfr2 NBR2 knock-out | AGAGGCTTTGGATGACTCTGCAAC |
| | GCGATGATCTCGGAGGAAAACTCC |

| | |
|---|---|
| Zfp281 knock-out | TGTGGAGAGGACGGCGTTATTTTT |
| | TGAAACCCATACTACACTGGCTGC |
| Nono Knock out | AGGTTTCCCTGCTTGTCTTTGTCT |
| | GCAGCAACGCCCTTAATTTCAACA |
| Nanog-iRFP670 | ACCCAGGGGTGACAAAGTATTCCAA |
| | GCATTTTCCGTAATGCGCGTGATCC |
| Nanog-sfGFP | ACCCAGGGGTGACAAAGTATTCCAA |
| | CGTTTGTAGCATCACCTTCACCCTC |
| Nanog-T2AmCherry | ACCCAGGGGTGACAAAGTATTCCAA |
| | TCGCCCTTGCTCACCATTGGCCCGGGATTCTCTTC |
| **q-RT-PCR primers** | |
| *Dusp6* | CTGCCATTAATGTGGCCATCCC |
| | GTGTTCTCATTCCAGTCGCTGC |
| *Nanog* | TGGTCCCCACAGTTTGCCTAGTTC |
| | CAGGTCTTCAGAGGAAGGGCGA |
| *Oct4* | GTGGAGGAAGCCGACAACAATGA |
| | CAAGCTGATTGGCGATGTGAG |
| *Sox2* | TTTTCTAGTCGGCATCACCG |
| | ACAAGAGAATTGGGAGGGGT |
| *Klf4* | GTGCAGCTTGCAGCAGTAAC |
| | AGCGAGTTGGAAAGGATAAAGTC |
| *Rex1* | CAGTCCAGAATACCAGAGTGGAA |
| | ACTCTAGGTATCCGTCAGGGAAG |
| *Fgfr2* | CCCTGCGGAGACAGGTAACAG |
| | AGCGTCAGCTTATCTCTGGGGA |
| *Fgfr1* | ACCCTGTAGCTCCCTACTGGAC |
| | TGGCATAGCGAACCTTGTAGCC |
| *Fgf4* | ACACGAGGGACAGTCTTCTGGA |
| | TAGGCGTTGTAGTTGTTGGGCA |
| *Fgfbp1* | CTAACCTCAAGCTGGTGAACCCC |
| | TCTCTAATGGCCATGGTCTGGGT |
| *Gapdh* | CAACGGCACAGTCAAGGCCGA |
| | CCCTTCAAGTGGGCCCCGG |
| *Spry2* | CCACCGATTGCTTGGAAGTTGG |
| | AGGTCTTGGCAGTGTGTTCACC |
| Pre-*Nanog-1* | AGCCCAGTACTCAGGCTTGT |
| | AGCATCACAACACGCACCT |
| Pre-*Nanog-2* | GCCAGCAGATGGCATAATTT |
| | TGATGGCAATGCTGAGGTTA |
| Pre-*Oct4* | GTCCCAGCTGGTGTGACTCT |
| | TCTTCTGCTTCAGCAGCTTG |
| Pre-*Fgf4* | GACTACCTGCTGGGCCTCAAAA |
| | TACTCAGCCCCCGAGACTACTAC |
| Pre-*Fgfr2* | CCCGTCCCTTCCCAAATCTGATA |
| | TCACCTTGGGTCAGGATAACAAG |
| Pre-*Fgfbp1* | GACTACCTGCTGGGCCTCAAAA |
| | TACTCAGCCCCCGAGACTACTAC |
| Pre-*Fgfr1* | CCCGTCCCTTCCCAAATCTGATA |
| | TCACCTTGGGTCAGGATAACAAG |
| **q-ChIP-PCR primers** | |

| | |
|---|---|
| Nanog 5.5 kb | GTGGGTGCACACAGAGAACAAC |
| | CTGAGAGCTCAGGCCCACAAAG |
| Nanog -4.9 kb | AACATTCCTTTCCCCACCCACA |
| | AAGAGGTGGCTGGTAGCCAAAA |
| Nanog -4.7 kb | TGGGGTAAACTTAAGGCTATGG |
| | AGCTCTAAGCCGGTTCTCATTT |
| Nanog -3.9 kb | CCCTACCTCTCCTGAGGTGTGA |
| | CATGCCTGAGGAAGTCAGAGGA |
| Nanog -3.4 kb | TGTAGCCCTTGGTTAGTCCGAG |
| | GGCAGGCATCACCAAAGTCATT |
| Nanog -1.9 kb | GGTTCAGTCAGGCTGGGCAAT |
| | CTGCTGCCACACTATCACTGTC |
| Nanog -1.0 kb | AGCCGACTTAAGCTGGGTTAGA |
| | TGCTCTAGCTGGTCCCAAACTC |
| Nanog -0.05 kb | TAGGGTAGGAGGCTTGAGGGG |
| | AAGTCAGAAGGAAGTGAGCCGC |
| Nanog +.5 kb | CCGGTGATACGTTGGCCTTCTA |
| | ACTGCCCCCGAACATATTCCAA |
| Nanog +1.4 kb | GTTAGGAATGAACGGGTGGGGA |
| | AGTAGACAGCCCTGAAAGCAGC |
| Fgf4 +3.5 kb | GCCCAGAACCCAATTTTTATGCAC |
| | CAAAGTCCCAGAGCCATTCCCTT |
| Fgf4 -3.0 kb | TTAGCTCGCTTCAGGGAATGCTT |
| | TTGCTGTCTGTAGCCTCCCATAA |
| Fgf4 -6.5 kb | CACAAAGGTCGCTTAAGTGGTGG |
| | ACACGATTTCCAGACTCCTCCAG |
| Fgf4 -6.9 kb | TTAGGCACCCAAAGGCAGAATTG |
| | GTCCTGTTATTCATGGCAGGGGA |
| Fgfr1-5kb | TGGCCTTGGATGAATTGTTGGC |
| | TTCCACCTCCCTTCAGGACACT |
| Fgfr1+2.5 kb | TGGGGTGGTGTCTCTTCCTTTCAG |
| | CAAGCCATTAGGGAGGGAGGCAA |
| Fgfbp1-1.4 kb | TCCAGTGTGTGTGGTAAACAGGT |
| | AACACTGCCTCTGGATGGTCTAC |
| Fgfr2 -2.5 kb | TTTTGTCCCACTTCTTGGGGC |
| | AATCTTCCACCAGCCTGGACTC |
| Fgfr2 -4.4 kb | AAACAACGTAACGCATCCACTGT |
| | TGCACAGATGACCTCTCGGAAC |

**SI References**


1. I. Chambers *et al.*, Nanog safeguards pluripotency and mediates germline development. **450**, 1230-1234 (2007).
2. D. A. Faddah *et al.*, Single-cell analysis reveals that expression of nanog is biallelic and equally variable as that of other pluripotency factors in mouse ESCs. **13**, 23-29 (2013).
3. T. Weber *et al.*, Increasing the efficiency of homology-directed repair for CRISPR-Cas9-induced precise gene editing in mammalian cells. *Nature biotechnology* **33**, 543-548 (2015).

4. O. Gafni *et al.*, Derivation of novel human ground state naive pluripotent stem cells. *Nature* **504**, 282-286 (2013).
5. N. Festuccia *et al.*, Esrrb is a direct Nanog target gene that can substitute for Nanog function in pluripotent cells. **11**, 477-490 (2012).
6. V. Karwacki-Neisius *et al.*, Reduced Oct4 expression directs a robust pluripotent state with distinct signaling activity and increased enhancer occupancy by Oct4 and Nanog. **12**, 531-545 (2013).
7. W.-W. Tee, S. S. Shen, O. Oksuz, V. Narendra, D. J. C. Reinberg, ERK activity promotes chromatin features and RNAPII phosphorylation at developmental promoters in mouse ESCs. **156**, 678-690 (2014).
8. C. Ma *et al.*, Nono, a bivalent domain factor, regulates Erk signaling and mouse embryonic stem cell pluripotency. **17**, 997-1007 (2016).